Int J Fract (2022) 238:35–56
https://doi.org/10.1007/s10704-022-00649-9

ORIGINAL PAPER

Conservation laws for arbitrary objectives with application to fracture resistant design

Chung-Shuo Lee · Chun-Pei Chen · Hung-Yun Lin · Ganesh Subbarayan

Received: 12 April 2021 / Accepted: 11 April 2022 / Published online: 11 July 2022
© The Author(s), under exclusive licence to Springer Nature B.V. 2022

Abstract In this paper, we pose a configurational optimization problem to derive the sensitivity of an arbitrary objective to arbitrary motions of one or more finite-sized heterogeneities inserted into a homogeneous domain. In the derivation, we pose an adjoint boundary value problem and utilize the adjoint fields as well as the definition of a generalized Eshelby energy-momentum tensor for arbitrary objectives to express the final result. The resulting sensitivity may be expressed as surface integrals with jump terms across the heterogeneity boundaries that vanish on homogeneous domains yielding generalized conservation laws for arbitrary objectives. We then derive the specific path-independent forms of the sensitivity of the objective to arbitrary translation, rotation or scaling of the inserted heterogeneities. We next illustrate the application of the derived sensitivities to specific objectives common to fracture mechanics as well as to structural optimization. The chosen objectives include strain energy, trade-off between structural compliance and mass, and an arbitrary objective defined entirely on the boundary of the domain. We show that for the strain energy objective, the derived sensitivities naturally yield the classical J-, L- and M-integrals of fracture mechanics. The theory is implemented within an Isogeometric computational framework for fracture modeling termed Enriched Isogeometric analysis (EIGA). The EIGA computational technique is used to optimally identify worst-case locations for line cracks that are inserted into the domain as well as to optimally mitigate the risk of fracture due to a crack at its worst-case location by sequentially inserting and optimizing the configurations of circular/elliptical stiff/soft inclusions.

Keywords Configurational optimization · Material derivative · Generalized conservation laws · Enriched IGA · Fracture resistant design

C.-S. Lee, C.-P. Chen, H.-Y. Lin · G. Subbarayan (✉)
School of Mechanical Engineering, Purdue University, West Lafayette, IN 47907, USA
e-mail: ganeshs@purdue.edu

1 Introduction

Linear Elastic Fracture Mechanics (LEFM) has served as a powerful tool for analyzing behaviors of solids in the presence of cracks. LEFM utilizes the concepts of Stress Intensity Factor (SIF 1957) and Energy Release Rate (ERR 1957) to characterize the near-tip singular stress field and the release of total potential energy associated with crack extension, respectively. These concepts together with their experimentally determined critical values have enabled engineers to assess the risk of crack growth in a wide variety of materials and structures. Further pioneering work led to the path-independent J-integral of Rice (1968) to evaluate ERR corresponding to self-similar extension of a line crack. Knowles and Sternberg (1972), motivated by the pioneering work of Eshelby (1956), showed that Rice's J-integral is one of a class of conservation laws leading to the J-, L-, and M-path-independent integrals corre-

sponding to uniform translation, rotation, or scaling of a homogeneous, elastostatic domain. Budiansky and Rice (1973) argued based on the mathematical form of rate of total potential energy that J-, L- and M-integrals correspond to ERRs associated with translation, rotation, and scaling of a void or crack. Although Rice's J-integral and its applications have been extensively investigated, there appear to be only a few studies (Budiansky and O'Connell 1976; Freund 1978; He and Hutchinson 1981; Herrmann and Herrmann 1981; Park and Earmme 1986; Chen 2001; Chang and Chien 2002) providing physical insights into the properties and uses of L- and M-integrals.

As mentioned, the path-independent J-, L- and M-integrals may also be interpreted as providing sensitivities with respect to the total potential energy of a crack to translation, rotation and scaling. This suggests that it may be possible to generalize the J-, L- and M-integrals to derive sensitivities with respect to an *arbitrary objective, of an arbitrary shaped heterogeneity* to translation, rotation and scaling. Such an approach is philosophically related to the shape design sensitivity analysis of heterogeneities in a continuum (Dems and Mroz 1983, 1984; Haug et al. 1986; Arora and Cardoso 1992; Sokolowski and Zolesio 1992; Arora 1993) that is widely studied in the context of shape optimization (see Pironneau 1984; Bennett and Botkin 1986).

Dems and Mroz (1986) first derived the variation of an arbitrary functional of stress, strain or displacement to translation, rotation or size variation of heterogeneities within a body. In general, the material derivative concept of continuum mechanics has been argued as being more intuitive for deriving the sensitivities with respect to shape parameters (Arora 1993). However, such an use of material derivative to derive general conservation laws with respect to arbitrary objectives of an arbitrary shaped heterogeneity to translation, rotation and scaling does not appear to exist in the prior literature. Therefore, in the first part of this work, we pose a configurational optimization problem with an arbitrary objective and derive the material derivative to optimally locate heterogeneities within a solid. We show that the derived material derivatives corresponding to translation, rotation and scaling are a generalization of the classical J-, L- and M-integrals for arbitrary objectives and for heterogeneities with arbitrary shapes. We show that the derived sensitivities naturally depend on a generalized Eshelby-Energy momentum tensor. We also derive the path-independent forms of the sensitivities.

One application of the derived sensitivities is to modify the structure with the goal of mitigating the risk of catastrophic fracture. Thus, in the second part of the study, we derive the sensitivities of common structural optimization objectives to arbitrary motions of one or more finite-sized heterogeneities (cracks, voids and inclusions) inserted into a domain. Such analytical derivatives of arbitrary objectives to configurational changes of arbitrary shaped heterogeneities do not appear to exist in the literature. Using the sensitivities numerically evaluated on path-independent integrals, we optimally configure the heterogeneities to either identify the critical location for a crack or to ensure superior fracture resistance. The goal of this second part of this study is closely related to recent studies where material arrangement to ensure fracture resistance of the structure has been explored (Russ and Waisman 2019; Xia et al. 2018; Da and Qian 2020; Russ and Waisman 2020). However, the present study differs from the above mentioned studies in that the approach maintains explicit, sharp boundaries of the heterogeneities as they are configured within the domain. In this sense, we utilize methods of shape optimal design than classical topology optimization based on homogenization (Bendsøe and Kikuchi 1988) or material density redistribution (Subbarayan Subbarayan). The cracks are also not regularized using the phase field method in the present study.

Although the present study does not consider nucleating heterogeneities, identifying the location for nucleating new heterogeneities, introducing an initial seed geometry at the site and optimizing its shape was carried out in the pioneering work of Eschenauer termed the "bubble method" (Eschenauer and Kobelev 1974). The mathematical field of topological derivative (Sokolowski and Zochowski 1999; Cea et al. 2000) for nucleating infinitesimal spherical holes in the domain represents a generalization of the theory behind the bubble method. Later, Lin and Subbarayan (2013) demonstrated that a configurational derivative associated with a finite sized heterogeneity will yield the classical topological derivative when reduced to the special case of infinitesimally small spherical inclusions or holes.

The numerical examples in the present study use a general isogeometric analysis (IGA 2005) framework based on Non-Uniform Rational B-Splines (NURBS) for optimal design in the presence of cracks. The earliest demonstrations of the use of NURBS basis functions for optimal design was by Renken and Subbarayan (2000) and by Natekar et al. (2004). Natekar et al. used Boolean compositions of primitive geometries of *identical dimension* to mathematically describe and analyze a complex geometry. Later, Tambat and Subbarayan (2012) developed enriched isogeometric analysis (EIGA) that enabled one to compose and analyze geometrically lower-dimensional features such as cracks or boundaries with known behavioral conditions on an underlying higher-dimensional domain. In this paper, we model cracks using EIGA. We implement general path-independent sensitivity calculation for arbitrary objectives and carryout optimal design in the presence of heterogeneities such as cracks, elliptical inclusions or voids. We solve numerical examples to (a) identify locations in a structure where a crack would cause the maximum damage and (b) the optimal arrangement of heterogeneities (voids/inclusions) that mitigate the influence of an existing crack.

The rest of the paper is organized as follows. We begin with the derivation of a generalized conservation law valid for an arbitrary objective function by posing a configuration optimization problem in Sect. 2, and deriving the material derivative of the Lagrangian as the optimality condition to the posed problem. The material derivative is then described using a generalized Eshelby energy-momentum tensor in Sect. 3. A surface integral form of the material derivative is derived in Sect. 4. The general material derivative is simplified for specific configurational changes of translation, rotation and scaling to yield the generalized conservation laws in Sect. 5. The special forms of the generalized conservation law for various objectives including strain energy and structural compliance are illustrated in Sect. 6. Several numerical examples are solved in Sect. 8 to illustrate the identification of worst-case configuration for a crack as well as mitigation of a crack through insertion of single as well as multiple heterogeneities. The results are discussed in Sect. 9, and the paper is concluded in Sect. 10.

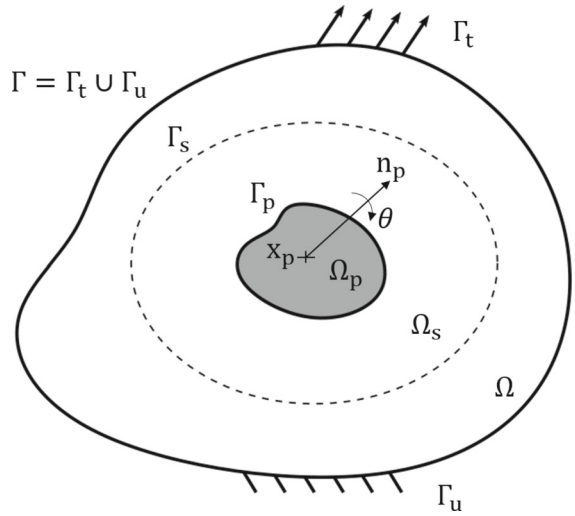

Fig. 1 Definition of the configurational optimization problem

2 Configurational optimization problem and configurational derivative

In this section, we derive the configurational derivative for an arbitrary objective function. We first introduce the configurational optimization problem, and derive configurational derivative by posing an adjoint boundary value problem.

Given a solid domain Ω containing a heterogeneity Ω_p as shown in Fig. 1, the linear elastic response within the domain at any instant of time t is governed by the principle of virtual work statement:

$$\int_\Omega \boldsymbol{\varepsilon} : \mathbf{C} : \boldsymbol{\varepsilon}^a \, d\Omega - \int_\Omega \mathbf{b} \cdot \mathbf{u}^a \, d\Omega - \int_{\Gamma_t} \mathbf{t} \cdot \mathbf{u}^a = 0 \quad (1)$$

where $\boldsymbol{\varepsilon}$ represents the infinitesimal strain tensor; $\boldsymbol{\varepsilon}^a$ and $\mathbf{u}^a$ are compatible virtual strains and displacements, respectively; $\mathbf{b}$ denotes the body forces prescribed in the domain; $\mathbf{t}$ denotes the surface tractions prescribed on the domain boundary; $\mathbf{C}$ is the fourth-rank tensor defining the linear elastic constitutive relation $\boldsymbol{\sigma} = \mathbf{C} : \boldsymbol{\varepsilon}$ between the stress $\boldsymbol{\sigma}$ and strain $\boldsymbol{\varepsilon}$ in the domain. Implicit in the above statement is the requirement that $\mathbf{u}^a = 0$ on the portion of the boundary Γ_u where displacement boundary conditions are applied. Also, Γ_t is the portion of boundary where tractions are prescribed, and the boundary of the domain is such that $\Gamma = \Gamma_u \cup \Gamma_t$ and $\Gamma_u \cap \Gamma_t = \emptyset$.

In general, the heterogeneity can be either stiff or soft. The goal of the configuration optimization problem is to optimally determine the reference location $\mathbf{x}_p$ of the heterogeneity, the orientation $\mathbf{n}_p$ of a reference axis passing through $\mathbf{x}_p$, and a rotation θ about the reference axis as well as the heterogeneity shape to achieve the greatest/least effect on a performance objective defined in the domain and/or on the boundary.

The configurational optimization problem is mathematically posed as the following instantaneous optimization problem: determine, at any instant, the position $\mathbf{x}_p(t)$ and axis orientation $\mathbf{n}_p(t)$, and rotation about the axis $\theta(t)$ to:

$$\begin{aligned}
&\text{minimize } f(t) = \int_\Omega \psi(\mathbf{u}, \boldsymbol{\varepsilon}, \xi; t)\, d\Omega + \int_\Gamma \phi(\mathbf{u}, \eta; t)\, d\Gamma \\
&\text{subject to } c(t) = \int_\Omega \boldsymbol{\sigma} : \boldsymbol{\varepsilon}^a\, d\Omega - \int_\Omega \mathbf{b}\cdot\mathbf{u}^a\, d\Omega - \int_\Gamma \mathbf{t}\cdot\mathbf{u}^a\, d\Gamma \\
&\qquad \mathbf{x}_p \subseteq \Omega_s \subset \Omega \\
&\qquad \|\mathbf{n}_p\| = 1
\end{aligned} \tag{2}$$

where ψ and ϕ are arbitrary design criteria evaluated at the instant of time t in the domain and its boundary, respectively; ξ and η are arbitrary design variables defined on the domain (such as the domain material cost) and boundary respectively that are not directly connected to the configurational variables $\mathbf{x}_p(t)$, $\mathbf{n}_p(t)$, and $\theta(t)$. All the strain and displacement terms as well as the design variables are allowed to be functions of time. The time may correspond to the physical time or a fictitious design time.

The Lagrangian corresponding to this problem is:

$$G(t) = f(t) - c(t) = \int_\Omega \bar{\psi}\, d\Omega + \int_\Gamma \bar{\phi}\, d\Gamma \tag{3}$$

where the usual Lagrange multiplier has been absorbed into the arbitrary, but compatible virtual displacements $\mathbf{u}^a$. Also, $\bar{\psi} = \psi - \boldsymbol{\sigma} : \boldsymbol{\varepsilon}^a + \mathbf{b}\cdot\mathbf{u}^a$ and $\bar{\phi} = \phi + \mathbf{t}\cdot\mathbf{u}^a$ and the arguments of the functions have been left out for ease of reading. The material time derivative of the lagrangian is the following

$$\begin{aligned}
\dot{G}(t) = &\int_\Omega \dot{\bar{\psi}}\, d\Omega + \int_\Gamma \dot{\bar{\phi}}\, d\Gamma + \int_\Omega \bar{\psi}(\nabla\cdot\mathbf{v})\, d\Omega \\
&+ \int_\Gamma \bar{\phi}(\nabla\cdot\mathbf{v} - \mathbf{n}\cdot\nabla\mathbf{v}\cdot\mathbf{n})\, d\Gamma
\end{aligned} \tag{4}$$

In the above equation, $\dot{\bar{\psi}}$ and $\dot{\bar{\phi}}$ can be simplified by introducing $\boldsymbol{\sigma}^a = \mathbf{C} : \boldsymbol{\varepsilon}^a - \frac{\partial\psi}{\partial\boldsymbol{\varepsilon}}$, $\mathbf{b}^a = \frac{\partial\psi}{\partial\mathbf{u}}$ and $\mathbf{t}^a = \frac{\partial\phi}{\partial\mathbf{u}}$:

$$\begin{aligned}
\dot{\bar{\psi}} = &\frac{\partial\psi}{\partial t} - \boldsymbol{\sigma} : \dot{\boldsymbol{\varepsilon}}^a - \boldsymbol{\sigma}^a : \dot{\boldsymbol{\varepsilon}} + \dot{\mathbf{b}}\cdot\mathbf{u}^a + \mathbf{b}\cdot\dot{\mathbf{u}}^a + \mathbf{b}^a \\
&\cdot\dot{\mathbf{u}} + \frac{\partial\psi}{\partial\xi}\dot{\xi}
\end{aligned} \tag{5}$$

$$\dot{\bar{\phi}} = \frac{\partial\phi}{\partial t} + \dot{\mathbf{t}}\cdot\mathbf{u}^a + \mathbf{t}\cdot\dot{\mathbf{u}}^a + \mathbf{t}^a\cdot\dot{\mathbf{u}} + \frac{\partial\phi}{\partial\eta}\dot{\eta} \tag{6}$$

Now, given $\dot{\boldsymbol{\varepsilon}} = \frac{1}{2}\left(\nabla\dot{\mathbf{u}}^T + \nabla\dot{\mathbf{u}}\right) - \frac{1}{2}\left(\nabla\mathbf{u}^T\cdot\nabla\mathbf{v}^T + \nabla\mathbf{v}\cdot\nabla\mathbf{u}\right)$, assuming $\dot{\mathbf{u}}$ and $\frac{1}{2}\left(\nabla\dot{\mathbf{u}}^T + \nabla\dot{\mathbf{u}}\right)$ are compatible, $\dot{\mathbf{u}}$ may be considered as a virtual displacement leading to the following adjoint boundary value problem for the solution to $\mathbf{u}^a$:

$$\begin{aligned}
&\int_\Omega \boldsymbol{\sigma}^a : \frac{1}{2}(\nabla\dot{\mathbf{u}}^T + \nabla\dot{\mathbf{u}})\, d\Omega - \int_\Omega \mathbf{b}^a\cdot\dot{\mathbf{u}}\, d\Omega \\
&- \int_{\Gamma_t} \mathbf{t}^a\cdot\dot{\mathbf{u}}\, d\Gamma = 0
\end{aligned} \tag{7}$$

where

$$\boldsymbol{\sigma}^a = \mathbf{C} : \boldsymbol{\varepsilon}^a - \frac{\partial\psi}{\partial\boldsymbol{\varepsilon}} \qquad in\ \Omega \tag{8}$$

$$\mathbf{b}^a = \frac{\partial\psi}{\partial\mathbf{u}} \qquad in\ \Omega \tag{9}$$

$$\dot{\mathbf{u}} = 0 \qquad on\ \Gamma_u \tag{10}$$

$$\mathbf{t}^a = \frac{\partial\phi}{\partial\mathbf{u}} \qquad on\ \Gamma_t \tag{11}$$

Similarly, given Eq. (1) and given $\dot{\boldsymbol{\varepsilon}}^a = \frac{1}{2}\left(\nabla\dot{\mathbf{u}}^{aT} + \nabla\dot{\mathbf{u}}^a\right) - \frac{1}{2}\left(\nabla\mathbf{u}^{aT}\cdot\nabla\mathbf{v}^T + \nabla\mathbf{v}\cdot\nabla\mathbf{u}^a\right)$, assuming $\dot{\mathbf{u}}^a$ and $\frac{1}{2}\left(\nabla\dot{\mathbf{u}}^{aT} + \nabla\dot{\mathbf{u}}^a\right)$ are compatible, terms in Eq. (4) can be further simplified as

$$\begin{aligned}
&\int_\Omega \dot{\bar{\psi}}\, d\Omega \\
&\quad + \int_\Gamma \dot{\bar{\phi}}\, d\Gamma \\
&= \int_\Omega \boldsymbol{\sigma} : (\nabla\mathbf{v}\cdot\nabla\mathbf{u}^a)\, d\Omega \\
&\quad + \int_\Omega \boldsymbol{\sigma}^a : (\nabla\mathbf{v}\cdot\nabla\mathbf{u})\, d\Omega \\
&\quad + \int_\Omega \left(\frac{\partial\psi}{\partial t} + \frac{\partial\psi}{\partial\xi}\dot{\xi}\right) d\Omega
\end{aligned} \tag{12}$$

$$+\int_\Gamma (\frac{\partial \phi}{\partial t}+\frac{\partial \phi}{\partial \eta}\dot{\eta})\, d\Gamma$$
$$+\int_\Omega \dot{\mathbf{b}}\cdot\mathbf{u}^a\, d\Omega+\int_\Gamma \dot{\mathbf{t}}\cdot\mathbf{u}^a\, d\Gamma$$

Thus, the material time derivative of the Lagrangian, Eq. (4), reduces to the following:

$$\begin{aligned}\dot{G}(t)=&\int_\Omega [\psi-\boldsymbol{\sigma}:\boldsymbol{\varepsilon}^a\\ &+\mathbf{b}\cdot\mathbf{u}^a](\nabla\cdot\mathbf{v})\, d\Omega+\int_\Omega \boldsymbol{\sigma}:(\nabla\mathbf{v}\cdot\nabla\mathbf{u}^a)\, d\Omega\\ &+\int_\Omega \boldsymbol{\sigma}^a:(\nabla\mathbf{v}\cdot\nabla\mathbf{u})\, d\Omega\\ &+\int_\Gamma [\phi+\mathbf{t}\cdot\mathbf{u}^a](\nabla\cdot\mathbf{v}-\mathbf{n}\cdot\nabla\mathbf{v}\cdot\mathbf{n})\, d\Gamma\\ &+\int_\Omega \dot{\mathbf{b}}\cdot\mathbf{u}^a\, d\Omega+\int_\Gamma \dot{\mathbf{t}}\cdot\mathbf{u}^a\, d\Gamma\\ &+\int_\Omega \left(\frac{\partial\psi}{\partial t}+\frac{\partial\psi}{\partial\xi}\dot{\xi}\right) d\Omega\\ &+\int_\Gamma \left(\frac{\partial\phi}{\partial t}+\frac{\partial\phi}{\partial\eta}\dot{\eta}\right) d\Gamma\end{aligned} \tag{13}$$

The time derivative $\dot{G}(t)$ is termed here as the *configurational derivative*. This derivative is identical to the material derivative of the objective $f(t)$ if the virtual work constraint $c(t)=0$ is satisfied at every instant.

3 Generalized Eshelby energy-momentum tensor for arbitrary objectives

In this section, we introduce a generalized Eshelby energy-momentum tensor $\boldsymbol{\Sigma}$, which is not only helpful to simplify Eq. (13), but also to derive the path independent integrals later. Gathering the terms in Eq. (13), we write

$$\begin{aligned}&\int_\Omega \left[\psi-\boldsymbol{\sigma}:\boldsymbol{\varepsilon}^a+\mathbf{b}\cdot\mathbf{u}^a\right](\nabla\cdot\mathbf{v})\, d\Omega\\ &+\int_\Omega \boldsymbol{\sigma}:(\nabla\mathbf{v}\cdot\nabla\mathbf{u}^a)\, d\Omega+\int_\Omega \boldsymbol{\sigma}^a:(\nabla\mathbf{v}\cdot\nabla\mathbf{u})\, d\Omega\\ =&\int_\Omega \Big[(\psi-\boldsymbol{\sigma}:\boldsymbol{\varepsilon}^a+\mathbf{b}\cdot\mathbf{u}^a)\mathbf{I}+\boldsymbol{\sigma}\cdot\nabla\mathbf{u}^{aT}+\boldsymbol{\sigma}^a\\ &\cdot\nabla\mathbf{u}^T\Big]:\nabla\mathbf{v}\, d\Omega=\int_\Omega \boldsymbol{\Sigma}:\nabla\mathbf{v}\, d\Omega\end{aligned} \tag{14}$$

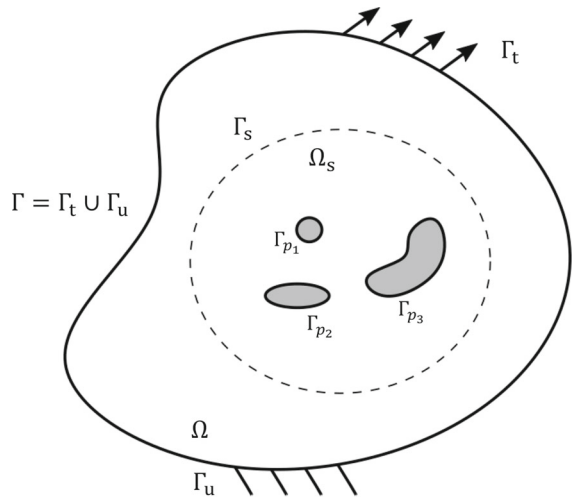

Fig. 2 Path integral with many heterogeneities

where, the generalized Eshelby energy-momentum tensor $\boldsymbol{\Sigma}$ is defined as,

$$\boldsymbol{\Sigma}=\left(\psi-\boldsymbol{\sigma}:\boldsymbol{\varepsilon}^a+\mathbf{b}\cdot\mathbf{u}^a\right)\mathbf{I}+\boldsymbol{\sigma}\cdot\nabla\mathbf{u}^{aT}+\boldsymbol{\sigma}^a\cdot\nabla\mathbf{u}^T \tag{15}$$

Thus, the configurational derivative of Eq. (13) can be stated using the Eshelby energy momentum tensor as

$$\begin{aligned}\dot{G}=&\int_\Omega \boldsymbol{\Sigma}:\nabla\mathbf{v}\, d\Omega+\int_\Gamma \left[\phi+\mathbf{t}\cdot\mathbf{u}^a\right]\\ &(\nabla\cdot\mathbf{v}-\mathbf{n}\cdot\nabla\mathbf{v}\cdot\mathbf{n})\, d\Gamma+\int_\Omega \dot{\mathbf{b}}\cdot\mathbf{u}^a\, d\Omega\\ &+\int_\Gamma \dot{\mathbf{t}}\cdot\mathbf{u}^a\, d\Gamma+\int_\Omega \left(\frac{\partial\psi}{\partial t}+\frac{\partial\psi}{\partial\xi}\dot{\xi}\right) d\Omega\\ &+\int_\Gamma \left(\frac{\partial\phi}{\partial t}+\frac{\partial\phi}{\partial\eta}\dot{\eta}\right) d\Gamma\end{aligned} \tag{16}$$

4 Simplification to a surface integral

We begin by observing that

$$\boldsymbol{\Sigma}:\nabla\mathbf{v}=\nabla\cdot(\boldsymbol{\Sigma}\cdot\mathbf{v})-(\nabla\cdot\boldsymbol{\Sigma})\cdot\mathbf{v} \tag{17}$$

Now, applying the divergence theorem, the first term on the right hand side of Eq. (17) can be expressed on a domain containing multiple heterogeneities (see Fig. 2)

as,

$$\int_{\Omega} \nabla \cdot (\mathbf{\Sigma} \cdot \mathbf{v})\, d\Omega = \sum_{i=1}^{N} \left(\int_{\Gamma_{p_i}} [\![\mathbf{n} \cdot \mathbf{\Sigma}]\!] \cdot \mathbf{v}\, d\Gamma \right) + \int_{\Gamma} \mathbf{n} \cdot \mathbf{\Sigma} \cdot \mathbf{v}\, d\Gamma \tag{18}$$

where, $\mathbf{v}$ is assumed continuous across Γ_p, and the jump term is defined as $[\![\bullet]\!] = [\bullet^+ + \bullet^-]$. Next, it is derived and shown in Appendix A.1 that

$$\nabla \cdot \mathbf{\Sigma} = -\boldsymbol{\varepsilon} : \nabla \mathbf{C} : \boldsymbol{\varepsilon}^a + \nabla \mathbf{b} \cdot \mathbf{u}^a \tag{19}$$

Thus, if $\nabla \mathbf{C} = 0$ and $\nabla \mathbf{b} = 0$ at a point in the domain, then we obtain the useful property,

$$\nabla \cdot \mathbf{\Sigma} = 0 \tag{20}$$

Next, to simplify the material derivative of Eq. (16), the following may be reasonable assumptions for most problems:

- $\mathbf{v} = 0$ and $\nabla \mathbf{v} = 0$ on Γ, assumed for convenience since $\mathbf{v}$ is arbitrary.
- $\mathbf{C}$ and $\mathbf{b}$ have no local spatial variation in Eq. (19), i.e., $\nabla \cdot \mathbf{\Sigma} = 0$
- Design criteria do not possess explicit dependence on design time t, i.e, $\frac{\partial \psi}{\partial t} = \frac{\partial \phi}{\partial t} = 0$.
- Applied body force in the domain and tractions on the boundary do not vary with design time, i.e., $\dot{\mathbf{b}} = \dot{\mathbf{t}} = 0$.
- ψ and ϕ do not depend on any arbitrary design variable, i.e., $\frac{\partial \psi}{\partial \xi} = \frac{\partial \phi}{\partial \eta} = 0$, or, alternatively, $\dot{\xi} = \dot{\eta} = 0$, i.e., ξ and η do not evolve at points in their respective domains.

Under these assumptions, using Eq. (17), the material derivative of Eq. (16) can be reduced to

$$\dot{G}(t) = \sum_{i=1}^{N} \left(\int_{\Gamma_{p_i}} [\![\mathbf{n} \cdot \mathbf{\Sigma}]\!] \cdot \mathbf{v}\, d\Gamma \right) \tag{21}$$

Clearly, on a homogeneous domain where the jump terms vanish, $\dot{G}(t) = 0$. Therefore, $\dot{G}(t)$ is a *conserved integral*.

Finally, using Eq. (18), the integration can be carried out in an arbitrary subdomain Ω_s and its boundary Γ_s (see Fig. 2) rather than evaluate the jump term:

$$\dot{G}(t) = \sum_{i=1}^{N} \left(\int_{\Gamma_{p_i}} [\![\mathbf{n} \cdot \mathbf{\Sigma}]\!] \cdot \mathbf{v}\, d\Gamma \right) = \int_{\Omega_s} \mathbf{\Sigma} : \nabla \mathbf{v}\, d\Omega - \int_{\Gamma_s} \mathbf{n} \cdot \mathbf{\Sigma} \cdot \mathbf{v}\, d\Gamma \tag{22}$$

The choice between using Eqs. (21) and (22) to evaluate the material derivative is one of computational accuracy and convenience.

5 Sensitivity to translation, rotation and scaling

In this section, we derive the forms of the configurational derivative corresponding to specific configurational changes of translation, rotation, and scaling.

We begin by considering a general transformation of the following form to describe the velocity in the domain Ω_s:

$$\mathbf{v} = \mathbf{A}(t) \cdot \mathbf{x} + \mathbf{c}(t) \tag{23}$$

where, $\mathbf{A}$ is a second-order tensor and $\mathbf{c}$ is a first-order tensor. The final result in their path-independent forms are presented below for succinctness, but the detailed derivation is included in Appendix A.

5.1 Translation

Translation of the heterogeneity is described by setting $\mathbf{v} \equiv \mathbf{c}$ and $\nabla \mathbf{v} \equiv 0$ in Ω_s, with $\mathbf{c}$ being a constant vector. Substituting the velocity into Eq. (22) we get:

$$\dot{G}_T = \sum_{i=1}^{N} \left(\int_{\Gamma_{p_i}} [\![\mathbf{n} \cdot \mathbf{\Sigma}]\!]\, d\Gamma \right) \cdot \mathbf{c} \tag{24}$$

$$= -\int_{\Gamma_s} \mathbf{n} \cdot \mathbf{\Sigma} \cdot \mathbf{c}\, d\Gamma \tag{25}$$

5.2 Rotation

Rotation is described by $\mathbf{v} = \mathbf{W}\mathbf{x} = \mathbf{w} \times \mathbf{x}$ and $\nabla \mathbf{v} = \mathbf{W}^T$ in Ω_s. Here, $\mathbf{W}$ is a constant anti-symmetric tensor

and $\mathbf{w}$ is the constant vorticity vector which defines $\mathbf{W}$. Substituting for velocity, Eq. (21) yields:

$$\dot{G}_R = \sum_{i=1}^{N} \left(\int_{\Gamma_{p_i}} \mathbf{x} \times [\![\mathbf{n} \cdot \boldsymbol{\Sigma}]\!] \, d\Gamma \right) \cdot \mathbf{w} \tag{26}$$

Now, under rotation, the first term on the right hand side of Eq. (22) is simplified in Appendix A.2 as

$$\begin{aligned} &\int_{\Omega_s} \boldsymbol{\Sigma} : \nabla \mathbf{v} \, d\Omega \\ &= \int_{\Omega_s} \left(\boldsymbol{\sigma} \cdot \boldsymbol{\varepsilon}^a + \boldsymbol{\sigma}^a \cdot \boldsymbol{\varepsilon} \right) : \mathbf{W}^T \, d\Omega \\ &\quad - \int_{\Gamma_s} \left(\mathbf{t}\mathbf{u}^a + \mathbf{t}^a \mathbf{u} \right) : \mathbf{W}^T \, d\Gamma \\ &\quad - \int_{\Omega_s} \left(\mathbf{b}\mathbf{u}^a + \mathbf{b}^a \mathbf{u} \right) : \mathbf{W}^T \, d\Omega \end{aligned} \tag{27}$$

For an isotropic material ($\boldsymbol{\sigma} = \lambda \, \mathrm{tr}(\boldsymbol{\varepsilon}) \, \mathbf{I} + 2\mu \, \boldsymbol{\varepsilon}$, $\boldsymbol{\sigma}^a = \lambda \, \mathrm{tr}(\boldsymbol{\varepsilon}^a) \, \mathbf{I} + 2\mu \, \boldsymbol{\varepsilon}^a - \frac{\partial \psi}{\partial \boldsymbol{\varepsilon}}$), the following further simplification is possible,

$$\left(\boldsymbol{\sigma} \cdot \boldsymbol{\varepsilon}^a + \boldsymbol{\sigma}^a \cdot \boldsymbol{\varepsilon} \right) : \mathbf{W}^T = \left[\lambda \left(\mathrm{tr}(\boldsymbol{\varepsilon}) \, \mathbf{I} \cdot \boldsymbol{\varepsilon}^a + \mathrm{tr}(\boldsymbol{\varepsilon}^a) \, \mathbf{I} \cdot \boldsymbol{\varepsilon} \right) + 2\mu \left(\boldsymbol{\varepsilon} \cdot \boldsymbol{\varepsilon}^a + \boldsymbol{\varepsilon}^a \cdot \boldsymbol{\varepsilon} \right) - \frac{\partial \psi}{\partial \boldsymbol{\varepsilon}} \cdot \boldsymbol{\varepsilon} \right] : \mathbf{W}^T = \left(-\frac{\partial \psi}{\partial \boldsymbol{\varepsilon}} \cdot \boldsymbol{\varepsilon} \right) : \mathbf{W}^T \tag{28}$$

since, the scalar product of the symmetric tensors with the anti-symmetric tensor $\mathbf{W}$ vanish. Furthermore, if $\frac{\partial \psi}{\partial \boldsymbol{\varepsilon}}$ is of the form $\frac{\partial \psi}{\partial \boldsymbol{\varepsilon}} = \mathbf{C} : \boldsymbol{\varepsilon} = p \, \mathbf{I} + q \, \boldsymbol{\varepsilon}$, where, $\mathbf{C}$ is a fourth rank isotropic tensor with major and minor symmetries, and p and q are invariant to rotation, then,

$$\left(\boldsymbol{\sigma} \cdot \boldsymbol{\varepsilon}^a + \boldsymbol{\sigma}^a \cdot \boldsymbol{\varepsilon} \right) : \mathbf{W}^T = 0 \tag{29}$$

Under these assumptions,

$$\int_{\Omega_s} \boldsymbol{\Sigma} : \nabla \mathbf{v} \, d\Omega = -\left[\int_{\Gamma_s} \left(\mathbf{t} \times \mathbf{u}^a + \mathbf{t}^a \times \mathbf{u} \right) \, d\Gamma + \int_{\Omega_s} \left(\mathbf{b} \times \mathbf{u}^a + \mathbf{b}^a \times \mathbf{u} \right) \, d\Omega \right] \cdot \mathbf{w} \tag{30}$$

and

$$\dot{G}_R = -\left\{ \int_{\Gamma_s} \left[\mathbf{x} \times (\mathbf{n} \cdot \boldsymbol{\Sigma}) + \mathbf{t} \times \mathbf{u}^a + \mathbf{t}^a \times \mathbf{u} \right] d\Gamma + \int_{\Omega_s} \left(\mathbf{b} \times \mathbf{u}^a + \mathbf{b}^a \times \mathbf{u} \right) d\Omega \right\} \cdot \mathbf{w} \tag{31}$$

5.3 Uniform scaling

Scaling results when $\mathbf{v} = \alpha \mathbf{x}$ and $\nabla \mathbf{v} = \alpha \mathbf{I}$ in Ω_s, where α determines the expansion rate. Substituting into Eq. (21) we get:

$$\dot{G}_S = \sum_{i=1}^{N} \left(\int_{\Gamma_{p_i}} [\![\mathbf{n} \cdot \boldsymbol{\Sigma}]\!] \cdot \mathbf{x} \, d\Gamma \right) \alpha \tag{32}$$

As with rotation, the first term on the right hand side of Eq. (22) is simplified in Appendix A.3 as

$$\int_{\Omega_s} \boldsymbol{\Sigma} : \nabla \mathbf{v} \, d\Omega = \alpha \left[d_m \int_{\Omega_s} \psi \, d\Omega - d_m \int_{\Gamma_s} \mathbf{t} \cdot \mathbf{u}^a \, d\Gamma + \int_{\Gamma_s} \left(\mathbf{t} \cdot \mathbf{u}^a + \mathbf{t}^a \cdot \mathbf{u} \right) \, d\Gamma + \int_{\Omega_s} \left(\mathbf{b} \cdot \mathbf{u}^a + \mathbf{b}^a \cdot \mathbf{u} \right) \, d\Omega \right] \tag{33}$$

where, d_m is the dimension of the problem (2 or 3). Thus, substituting into Eq. (22), we obtain,

$$\dot{G}_S = -\left[\int_{\Gamma_s} (\mathbf{n} \cdot \boldsymbol{\Sigma} \cdot \mathbf{x} - \mathbf{t} \cdot \mathbf{u}^a - \mathbf{t}^a \cdot \mathbf{u}) \, d\Gamma + d_m \left(\int_{\Gamma_s} \mathbf{t} \cdot \mathbf{u}^a \, d\Gamma - \int_{\Omega_s} \psi \, d\Omega \right) - \int_{\Omega_s} (\mathbf{b} \cdot \mathbf{u}^a + \mathbf{b}^a \cdot \mathbf{u}) \, d\Omega \right] \alpha \tag{34}$$

6 Examples of objective functions for configurational optimization

In this section, we illustrate the forms of the configurational derivative for various objectives. In general, for any choice of objective function, one needs to solve the adjoint boundary value problem in Eq. (7) to determine $\boldsymbol{\sigma}^a$, $\boldsymbol{\varepsilon}^a$, and $\mathbf{u}^a$. Using these adjoint quantities, the generalized Eshelby energy-momentum tensor, Eq. (15), is evaluated. Substituting the Eshelby energy-momentum tensor into Eqs. (25), (31) and (34), one obtains the

appropriate configurational derivatives. In the forms derived below, we assume the elasticity tensor $\mathbf{C}$ to be homogeneous and isotropic as required for Eq. (20) and Eq. (29).

6.1 Strain energy

Choosing strain energy as the objective, that is, setting $\psi = \frac{1}{2}\boldsymbol{\varepsilon} : \mathbf{C} : \boldsymbol{\varepsilon}$, $\phi = 0$, and $\mathbf{b} = 0$, the boundary conditions of the adjoint boundary value problem Eqs. (8), (9), (10) and (11) yields:

$$\boldsymbol{\sigma}^a = \mathbf{C} : (\boldsymbol{\varepsilon}^a - \boldsymbol{\varepsilon}),\ \mathbf{b}^a = 0,\ \mathbf{t}^a = 0 \tag{35}$$

As a result of the above conditions, the adjoint boundary value problem Eq. (7) becomes $\int_\Omega \boldsymbol{\varepsilon} : \boldsymbol{\sigma}^a \, d\Omega = 0$, which yields the following local conditions:

$$\boldsymbol{\sigma}^a = 0,\ \boldsymbol{\varepsilon}^a = \boldsymbol{\varepsilon},\ \mathbf{u}^a = \mathbf{u} \tag{36}$$

Substituting the adjoint solution into Eqs. (15), (25), (31) and (34) one obtains:

$$\boldsymbol{\Sigma} = -\psi \mathbf{I} + \boldsymbol{\sigma} \cdot \nabla \mathbf{u}^T \tag{37}$$

$$\dot{G}_T = \left\{ \int_{\Gamma_s} \left[\psi \mathbf{n} - \mathbf{t} \cdot \nabla \mathbf{u}^T \right] d\Gamma \right\} \cdot \mathbf{c} \tag{38}$$

$$\dot{G}_R = \left\{ \int_{\Gamma_s} \left[\psi (\mathbf{x} \times \mathbf{n}) - \mathbf{x} \times (\mathbf{t} \cdot \nabla \mathbf{u}^T) - \mathbf{t} \times \mathbf{u} \right] d\Gamma \right\} \cdot \mathbf{w} \tag{39}$$

$$\dot{G}_S = \left\{ \int_{\Gamma_s} \left[\psi (\mathbf{n} \cdot \mathbf{x}) - \mathbf{t} \cdot \nabla \mathbf{u}^T \cdot \mathbf{x} - (\frac{d_m - 2}{2}) \mathbf{t} \cdot \mathbf{u} \right] d\Gamma \right\} \alpha \tag{40}$$

The integrals within the curly braces in the above sensitivities are identical to the classical $J-$, $L-$ and $M-$integrals. In other words, the classical integrals are the solution to the more general configurational optimization problem when the chosen objective is the strain energy.

6.2 Trade-off between compliance and mass

Structural compliance is a common objective during design optimization. We next consider an objective that may be considered as a trade-off between structural compliance and mass: $\psi = (1-w)\boldsymbol{\varepsilon} : \mathbf{C} : \boldsymbol{\varepsilon} + w\rho = (1-w)\psi_\varepsilon + w\psi_\rho$, $\phi = 0$, and $\mathbf{b} = 0$. Here, ρ is the mass density of the inclusion, the parameter w represents user preference for either the compliance or the mass, and for various values of w, one obtains the Pareto-optimal family of non-dominated solutions. Following the procedure adopted before, the boundary conditions of the adjoint boundary value problem Eqs. (8), (9), (10) and (11) yield:

$$\boldsymbol{\sigma}^a = \mathbf{C} : [\boldsymbol{\varepsilon}^a - 2(1-w)\boldsymbol{\varepsilon}],\ \mathbf{b}^a = 0,\ \mathbf{t}^a = 0 \tag{41}$$

Again, the adjoint boundary value problem becomes $\int_\Omega \boldsymbol{\varepsilon} : \boldsymbol{\sigma}^a \, d\Omega = 0$, which yields the local conditions:

$$\boldsymbol{\varepsilon}^a = 2(1-w)\boldsymbol{\varepsilon},\ \mathbf{u}^a = 2(1-w)\mathbf{u},\ \boldsymbol{\sigma}^a = 0 \tag{42}$$

Now, substituting the adjoint solution into Eq. (15) gives:

$$\boldsymbol{\Sigma} = -(1-w)\left[(\boldsymbol{\varepsilon} : \mathbf{C} : \boldsymbol{\varepsilon})\mathbf{I} - 2\boldsymbol{\sigma} \cdot \nabla \mathbf{u}^T \right] + w\rho\mathbf{I} \tag{43}$$

$$= -(1-w)\boldsymbol{\Sigma}_\varepsilon + w\boldsymbol{\Sigma}_\rho \tag{44}$$

Given the above split in the Eshelby energy momentum tensor, to derive the sensitivities in this problem, it is convenient to rewrite Eq. (22) as:

$$\dot{G}(t) = -(1-w)\left[\int_{\Omega_s} \boldsymbol{\Sigma}_\varepsilon : \nabla \mathbf{v} \, d\Omega - \int_{\Gamma_s} \mathbf{n} \cdot \boldsymbol{\Sigma}_\varepsilon \cdot \mathbf{v} \, d\Gamma \right] + w \sum_{i=1}^{N} \left(\int_{\Gamma_{p_i}} [\![\mathbf{n} \cdot \boldsymbol{\Sigma}_\rho]\!] \cdot \mathbf{v} \, d\Gamma \right) \tag{45}$$

Now, if the densities are constant on either side of the particle boundary Γ_{p_i}, then,

$$\int_{\Gamma_{p_i}} [\![\mathbf{n}\rho]\!] \, d\Gamma = \int_{\Gamma_{p_i}} \mathbf{x} \times [\![\mathbf{n}\rho]\!] \, d\Gamma = 0 \tag{46}$$

This is as expected since there is no change in the mass of the structure due to translation or rotation of the heterogenieties. Thus, the sensitivities to translation, rotation and scaling for this problem are:

$$\dot{G}_T = \left\{ (1-w) \int_{\Gamma_s} \mathbf{n} \cdot \boldsymbol{\Sigma}_\varepsilon \, d\Gamma \right\} \cdot \mathbf{c} \tag{47}$$

$$\dot{G}_R = \left\{ (1-w) \int_{\Gamma_s} [\mathbf{x} \times (\mathbf{n} \cdot \boldsymbol{\Sigma}_\varepsilon) - 2\mathbf{t} \times \mathbf{u}] \, d\Gamma \right\} \cdot \mathbf{w} \tag{48}$$

$$\dot{G}_S = \left\{ (1-w) \int_{\Gamma_s} [\mathbf{n} \cdot \mathbf{\Sigma}_\varepsilon \cdot \mathbf{x} - (d_m - 2)\mathbf{t} \cdot \mathbf{u}] \, d\Gamma + w \sum_{i=1}^{N} \int_{\Gamma_{p_i}} [\![\mathbf{n}\rho]\!] \cdot \mathbf{x} \, d\Gamma \right\} \alpha \tag{49}$$

6.3 An arbitrary boundary objective function

Finally, we consider an objective that is defined only on the boundary $\psi = 0$, $\phi = \mathbf{n} \cdot \mathbf{A} \cdot \mathbf{u}$, and $\mathbf{b} = 0$, with $\mathbf{A}$ being a symmetric second rank tensor. If $\mathbf{A}$ were to be the stress tensor at the boundary with the normal $\mathbf{n}$, then the boundary objective may be interpreted as the potential of the applied tractions, which is related to structural compliance. For this objective, the boundary conditions for the adjoint problem become

$$\boldsymbol{\sigma}^a = \mathbf{C} : \boldsymbol{\varepsilon}^a, \ \mathbf{b}^a = 0, \ \mathbf{t}^a = \mathbf{A} \cdot \mathbf{n} \tag{50}$$

and the adjoint boundary value problem is $\int_\Omega \boldsymbol{\varepsilon} : \boldsymbol{\sigma}^a \, d\Omega = \int_{\Gamma_t} \mathbf{n} \cdot \mathbf{A} \cdot \mathbf{u} \, d\Gamma$, which yields the following solution:

$$\boldsymbol{\sigma}^a = \mathbf{A}, \ \boldsymbol{\varepsilon}^a = \mathbf{C}^{-1} : \mathbf{A}, \ \boldsymbol{\sigma} = \mathbf{A}, \ \boldsymbol{\varepsilon} = \mathbf{C}^{-1} : \mathbf{A} \tag{51}$$

Substituting the adjoint solution into Eqs. (15), (25), (31) and (34) we get:

$$\mathbf{\Sigma} = -(\mathbf{A} : \boldsymbol{\varepsilon}) \mathbf{I} + 2\mathbf{A} \cdot \nabla \mathbf{u}^T \tag{52}$$

$$\dot{G}_T = -\left\{ \int_{\Gamma_s} \mathbf{n} \cdot \mathbf{\Sigma} \, d\Gamma \right\} \cdot \mathbf{c} \tag{53}$$

$$\dot{G}_R = -\left\{ \int_{\Gamma_s} [\mathbf{x} \times (\mathbf{n} \cdot \mathbf{\Sigma}) + 2\mathbf{t} \times \mathbf{u}] \, d\Gamma \right\} \cdot \mathbf{w} \tag{54}$$

$$\dot{G}_S = -\left\{ \int_{\Gamma_s} [\mathbf{n} \cdot \mathbf{\Sigma} \cdot \mathbf{x} + (d_m - 2)\mathbf{t} \cdot \mathbf{u}] \, d\Gamma \right\} \alpha \tag{55}$$

7 Isogeometric enriched field approximations for modeling of heterogeneous structures containing cracks

An isogeometric analysis computational procedure (Hughes et al. 2005; Natekar et al. 2004) is used in the numerical examples described later to carryout fracture resistant design. Specifically, isogeometric enrichments of cracks or other heterogeneities embedded in the domain, termed enriched isogeometric analysis (Tambat and Subbarayan (2012)) is used. The computational methodology is briefly described below.

Boundaries with specified behavior, phase boundaries, crack surfaces or singular points are, geometrically speaking, lower-dimensional features relative to two- or three-dimensional geometrical domains. Often, the distinguishing characteristics of the behavior at these features are known *a priori* and may be exploited to enrich isogeometric models. Motivated by this observation, geometrically explicit, but behaviorally implicit enrichments (meaning enrichments on geometries with explicitly known boundaries) of boundary conditions, discontinuities, and singularities were constructed by Tambat and Subbarayan (2012). In EIGA, the behavioral approximation is constructed to form a partition of unity as follows:

$$f(\mathbf{x}) = \left(1 - \sum_{i=1}^{n_e} w_i(\mathbf{x})\right) f_\Omega(\mathbf{x}) + \sum_{i=1}^{n_e} w_i(\mathbf{x}) f_{\Gamma_i}(P(\mathbf{x})) \tag{56}$$

where f_Ω is the continuous approximation associated with the underlying domain Ω and f_{Γ_i} is the enrichment approximation defined isoparametrically on the ith external/internal boundary Γ_i. Not only can the enrichment f_{Γ_i} be a known function to apply boundary/interface conditions, it may also contain unknowns corresponding to the *a priori* knowledge of local behavior. Also, to infer the influence of the enrichment at a spatial location $\mathbf{x}$, a projection $P(\mathbf{x})$ is necessary to map the spatial point to the corresponding external/internal boundary Γ_i. The influence of the enriching field must decay with distance from the enriching geometrical entity, and therefore, the weight fields are required to be monotonically decreasing functions of distance. Here, a cubic function of the form given below is used although other choices are possible.

$$w\left(\frac{d}{d_0}\right) = \begin{cases} 1 - 3\left(\frac{d}{d_0}\right)^2 + 2\left(\frac{d}{d_0}\right)^3 & \text{for} \quad \frac{d}{d_0} \le 1 \\ 0 & \text{for} \quad \frac{d}{d_0} > 1 \end{cases} \tag{57}$$

where d is a monotonic measure of distance from the enriching geometry, d_0 is the maximum influence (or cutoff) distance from the external/internal boundary.

The EIGA formulation adopted here for modeling cracks is based on Chen et al. (2021). The displacement field is discontinuous across the crack face and may be described by enriched displacements fields from crack faces ($\mathbf{u}_{f_0}$ and $\mathbf{u}_f$) and crack tips ($\mathbf{u}_{t_0}$ and $\mathbf{u}_t$) as following:

$$\mathbf{u} = w_c\mathbf{u}_c + w_f\left(\mathbf{u}_{f_0} + H(\mathbf{x})\mathbf{u}_f\right) + w_t\left(\mathbf{u}_{t_0} + \mathbf{u}_t\right) \quad (58)$$

where $\mathbf{u}_c$ is the displacement associated with underlying domain, $\mathbf{u}_{f_0}$ is the displacement associated with crack face, $\mathbf{u}_f$ is the measure of opening of the crack, $\mathbf{u}_{t_0}$ is the displacement associated with crack tips, and $\mathbf{u}_t$ is the asymptotic displacement. $H(\mathbf{x})$ is the Heaviside function that takes the value of 1 on one side of the crack face and -1 on the other side to create a discontinuity across the crack.

The general solution for asymptotic displacement are given in Seweryn and Molski (1996); Luo and Subbarayan (2007) and can be express as a matrix-vector multiplication by the basis function $[\mathbf{N}_t]$ and unknowns $\{\mathbf{v}_t\}$:

$$\mathbf{u}_t = \begin{Bmatrix} \mathbf{u}_r \\ \mathbf{u}_\theta \end{Bmatrix} = [\mathbf{N}_t]\{\mathbf{v}_t\} = r^\lambda \begin{bmatrix} \cos(1+\lambda)\theta & \sin(1+\lambda)\theta & \cos(1-\lambda)\theta & \sin(1-\lambda)\theta \\ -\sin(1+\lambda)\theta & \cos(1+\lambda)\theta & -\frac{\kappa+\lambda}{\kappa-\lambda}\sin(1-\lambda)\theta & \frac{\kappa+\lambda}{\kappa-\lambda}\cos(1-\lambda)\theta \end{bmatrix} \begin{Bmatrix} A \\ B \\ C \\ D \end{Bmatrix} \quad (59)$$

where the four independent constants A, B, C, D and the eigenvalue λ are obtained after applying the boundary conditions. The eigenvalue for a crack under Mode I loading is $\lambda = \frac{1}{2}$ Seweryn and Molski (1996). κ is the Kolosov constant which has a value $3 - 4\nu$ under plane strain condition, and $(3-\nu)/(1+\nu)$ under plane stress condition, with ν being the Poisson ratio. The weight terms in Eq. (58) satisfy $w_c + w_f + w_t = 1$ everywhere in the domain. Fig. 3 shows the distribution of weight function contours around a line crack. The weight functions monotonically reduce from 1 to 0 in the vicinity of interface that allows enriched field approximation of a crack. In general, the weights w_f and w_t correspond to lower-dimensional enrichments and are such that:

$$w_\Gamma = w_f + w_t \quad (60)$$

$$w_c = 1 - w_\Gamma \quad (61)$$

8 Numerical examples

In this section, several numerical examples are solved. The fracture-resistant design demonstrated here unifies the assessment of risk (worst-case location of crack that leads to the largest value of the objective function) as well as the mitigation strategy (locations of stiffeners or voids to minimize the objective).

8.1 Configurational optimization of a line crack

First, numerical examples using both a domain objective function and a boundary objective function are presented to illustrate both the worst-case and the best-case configurations (location and orientation) of a line crack inserted into a homogeneous plate. The mathematical forms of the chosen objective functions were:

$$f_\Omega = \int_\Omega \psi \, d\Omega = \int_\Omega \frac{1}{2}\boldsymbol{\varepsilon} : \mathbf{C} : \boldsymbol{\varepsilon} \, d\Omega \quad (62)$$

$$f_\Gamma = \int_\Gamma \phi \, d\Gamma = \int_\Gamma \mathbf{n} \cdot \mathbf{A} \cdot \mathbf{u} \, d\Gamma \quad (63)$$

where, $\mathbf{A} = [(-|x - 0.5| + 0.5)y]\,\mathbf{I}$.

The plate geometry as well as the selected crack length ($2a = 0.2$), material properties (Young's modulus $E = 1$ and Possion's ratio $\nu = 0.3$), loading and boundary conditions are illustrated in Fig. 4.

At every iteration, the chosen objective function (f_Ω and f_Γ was evaluated on a fixed boundary Γ_s close to the external boundary of the plate, illustrated by a dashed line in the figure. Using the sensitivities in Eqs. (38) and (53), at each iteration, the steepest ascent/descent direction was identified to

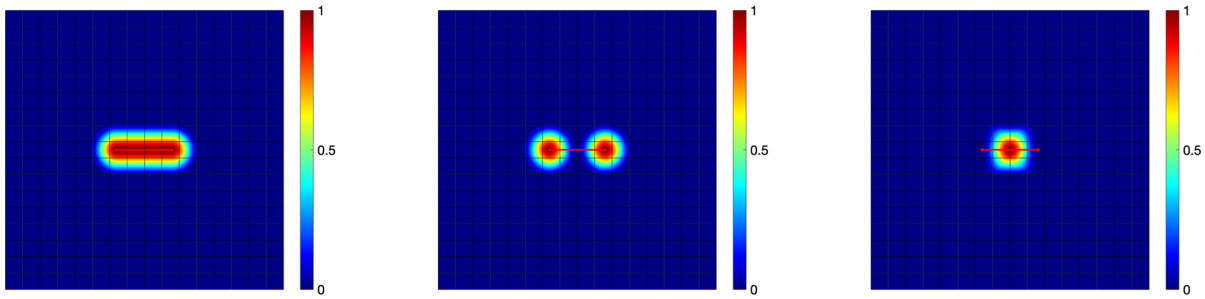

Fig. 3 The weight function contours of **a** w_Γ **b** w_t **c** w_f

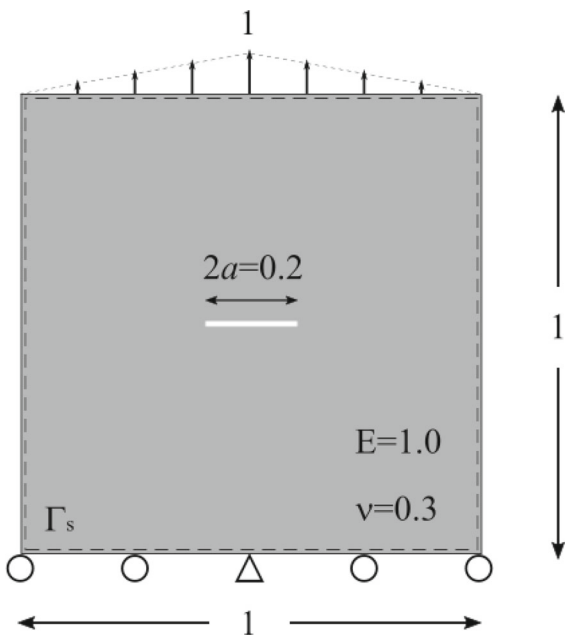

Fig. 4 Geometry, loading and boundary conditions for illustrating the identification of the worst or best configurations for a crack in a structure. The dashed contour represents the integration path for the sensitivities

increase/decrease the objective function. The initial value of the function was used to normalize the objective during the iterations to assure better scaling and numerical stability in step size determination. A minimum distance ($d = 0.1$) between the crack and the boundary was enforced as a stop criterion to prevent the moving crack from intersecting the boundary. The iterations were continued until the worst or the best configuration for the crack was identified. The worst configuration for the crack was observed to be at the center of the plate in x direction, but near the top boundary in y direction regardless of the chosen objective or the initial location of the crack, as shown in Fig. 5a. The increase in the value of the objectives with each iteration is plotted in Fig. 5b. The least harmful (or best) location for the crack required a move away from the boundary with the loading in all cases. But, the optimal location along the x direction was sensitive to the initial location as shown in Fig. 6. The decrease in the value of the objective with iteration count is plotted in Fig. 6b.

8.2 Optimal mitigation of a crack through configuration of an inserted heterogeneity

A strategy of inserting and optimizing the configuration of a circular or elliptical heterogeneity (void or inclusion) to mitigate the risk due to a crack is next illustrated. Four types of configurational changes are illustrated: (a) translation only (b) scaling only (c) both translation and rotation (meaningful only for elliptical heterogeneities) and (d) both scaling and rotation (meaningful only for elliptical heterogeneities). The geometry, loading and boundary conditions are identical to that used earlier in Fig. 4 except for the initial crack and heterogeneity locations. In all simulations, the crack was held fixed at the worst-case configuration identified earlier as (0.5,0.9), shown in Fig. 5. The circular/elliptical void or inclusion was then optimized to mitigate the influence of the crack. The void was modeled as a soft material with an elastic modulus of $E = 10^{-3}$, and the elastic modulus of the stiff inclusion was chosen as $E = 10^3$. As before, the value of the strain energy in the initial configuration, U_0, was used to normalize the objective. At each iteration, $\dot{G}_T$,

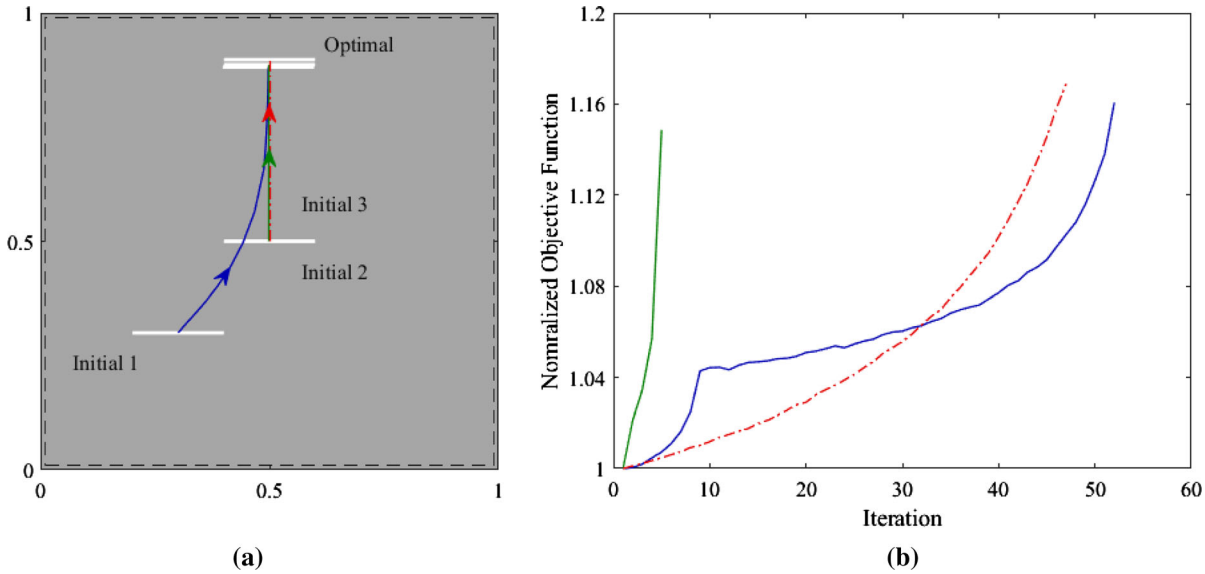

Fig. 5 Worst-case configurations for the strain energy or the boundary objective function of a line crack inserted into a square plate: **a** Optimal locations of the crack obtained using the two objective functions. **b** Increase in the value of the objective with the iteration count. Solid lines correspond to the strain energy objective iterates starting from the two different initial locations. Dash-dotted line corresponds to the boundary objective function

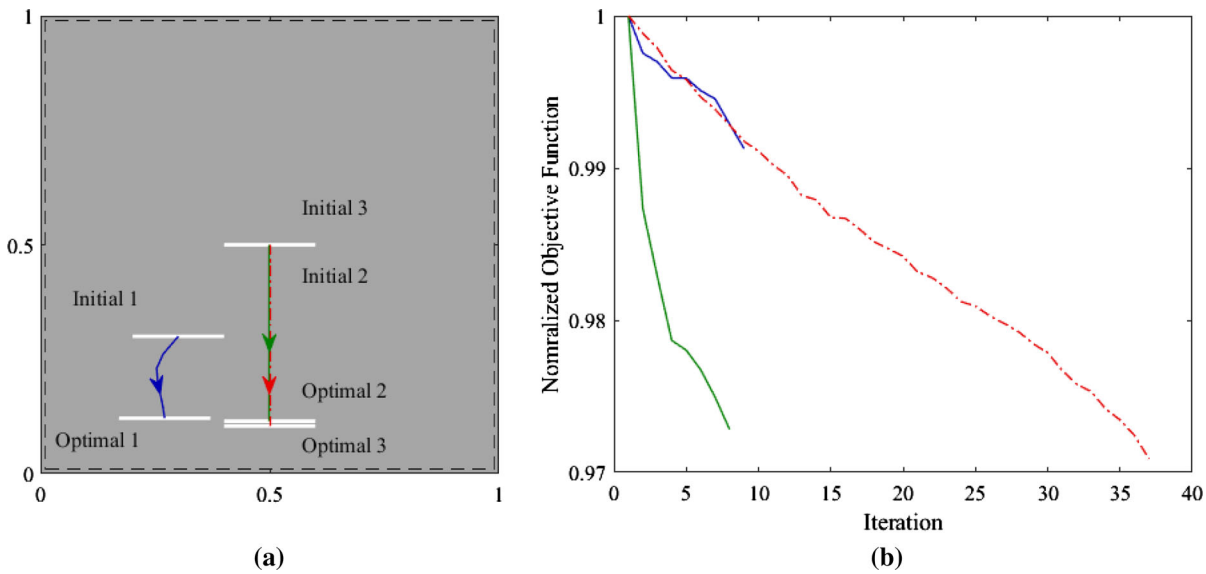

Fig. 6 Best-case configurations for the strain energy or the boundary objective function of a line crack inserted into a square plate: **a** Optimal locations of the crack obtained using the two objective functions. **b** Decrease in the value of the objective with the iteration count. Solid lines correspond to the strain energy objective iterates starting from the two different initial locations. Dash-dotted line corresponds to the boundary objective function

$\dot{G}_R$ and $\dot{G}_S$ in Eq. (38), Eq. (39) and Eq. (40) were evaluated on a circular path Γ_s that was the largest dimension of the heterogeneity plus a small offset distance (0.04 for circle and 0.064 for ellipse). This choice of circular path was convenient for evaluating the configurational derivatives for a rotating elliptical void or inclusion at all intermediate iterations as the configuration of the heterogeneity changed. The iterations were stopped when any of the following conditions was smaller than its preset criterion: (a) the difference in strain energy between two iterations (b) the distance between the void/inclusion and the crack tips (c) the distance between the void/inclusion and the boundary.

The optimal configurations for a circular void/inclusion with only translation to mitigate the influence of the crack are illustrated in Fig. 7 and Fig. 8. The optimal configurations of the elliptical void/inclusion with only translation being allowed from the initial configuration are illustrated in Figs. 9 and 10. The optimal configurations for a circular void/inclusion with only scaling to mitigate the influence of the crack are illustrated in Figs. 11 and 12. The optimal configurations when both translation and rotation of the introduced heterogeneity are allowed are illustrated in Figs. 13 and 14. The optimal configurations when both scaling and rotation of the introduced heterogeneity are allowed are illustrated in Figs. 15 and 16.

To minimize the strain energy in the domain, the void tended to move away from the crack (Figs. 7a, 9a and 13a) and to be as small as possible (Figs. 11a and 15a) as expected intuitively. The inclusion, on the other hand, tended to move closer to the crack tips (Figs. 8a, 10a and 14a) and to be as large as possible (Figs. 12a and 16a) to mitigate the crack. The optimal orientation of both the void and the inclusion tended to be aligned with the loading direction and perpendicular to the line crack. The solutions were in general non-unique and depended on the initial location of the introduced heterogeneity.

8.3 Optimal mitigation of a crack through insertion and configuration of multiple heterogeneities

Considering multiple heterogeneities within the domain, two mitigations are illustrated: (a) identifying the location of the crack with least risk for a given set of heterogeneities (b) optimizing the configuration of multiple heterogeneities for a given location of the crack. The geometry, loading and boundary conditions are identical to those used earlier and shown in Fig. 4. Four heterogeneities (two voids and two inclusions) and a line crack are modeled in the two cases. In the case where the location of the crack with least risk is identified, the crack is only translated. In the second case, three of the four inserted heterogeneities are allowed to translate, rotate, and uniformly scale, while one elliptical inclusion is only allowed to translate and rotate. The opimal configuration of the heterogeneities is achieved using Eq. (21) and (22). The results of the optimization are shown in Figs. 17 and 18. In these two cases, the same trends may be observed: (a) risk is mitigated when the crack is moved away from loading (b) voids tend to move away from the crack and will shrink to be as small as possible (c) inclusions tend to get closer to crack tips and to be as large as possible.

9 Discussion

In Sect. 8, numerical examples were solved to illustrate the optimal configuration of either a single inserted heterogeneity or multiple heterogeneities in the presence of a line crack. During the course of optimization, the heterogeneities may merge to create a new heterogeneity. While this is theoretically permissible, the numerical solution procedure however needs to be adapted to consider the configuration of the merged heterogeneity. The new merged entity requires one to define a new integration path for calculating the sensitivities. The numerical solution challenge is illustrated in Fig. 19. When two heterogeneities are in close proximity, as shown in Fig. 19a, smaller steps should be applied to prevent the two heterogeneities from overlapping suddenly. When the two heterogeneities merge, as shown in Fig. 19b, a new integral path is needed for this merged heterogeneity.

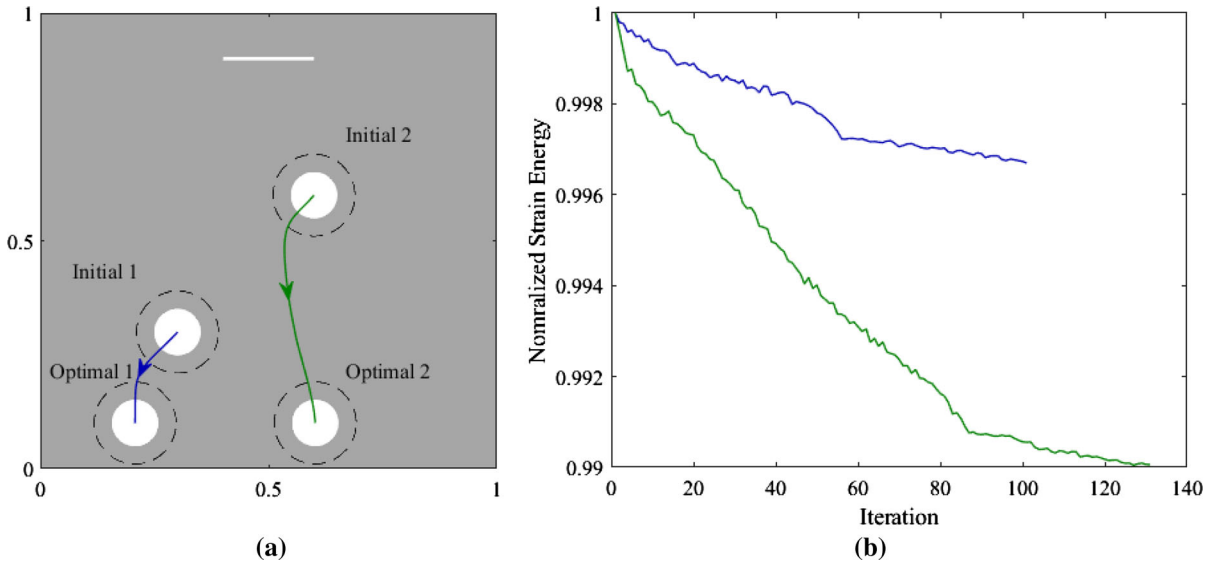

Fig. 7 Optimal configuration of a circular void inserted into the plate with a crack: **a** Optimal locations of the void starting from different initial locations. The dashed contour enclosing the voids represents the integration path for the sensitivities. **b** Strain energy decrease with iterations

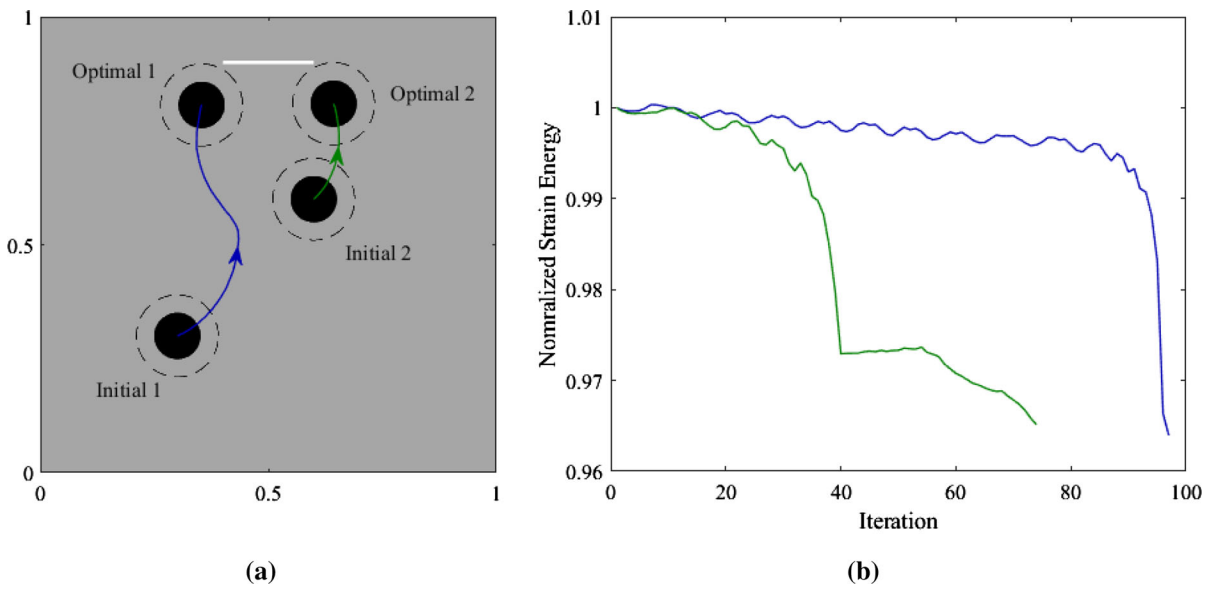

Fig. 8 Optimal configuration of a circular inclusion inserted into the plate with a crack: **a** Optimal locations of the inclusion starting from different initial locations. **b** Strain energy decrease with iterations

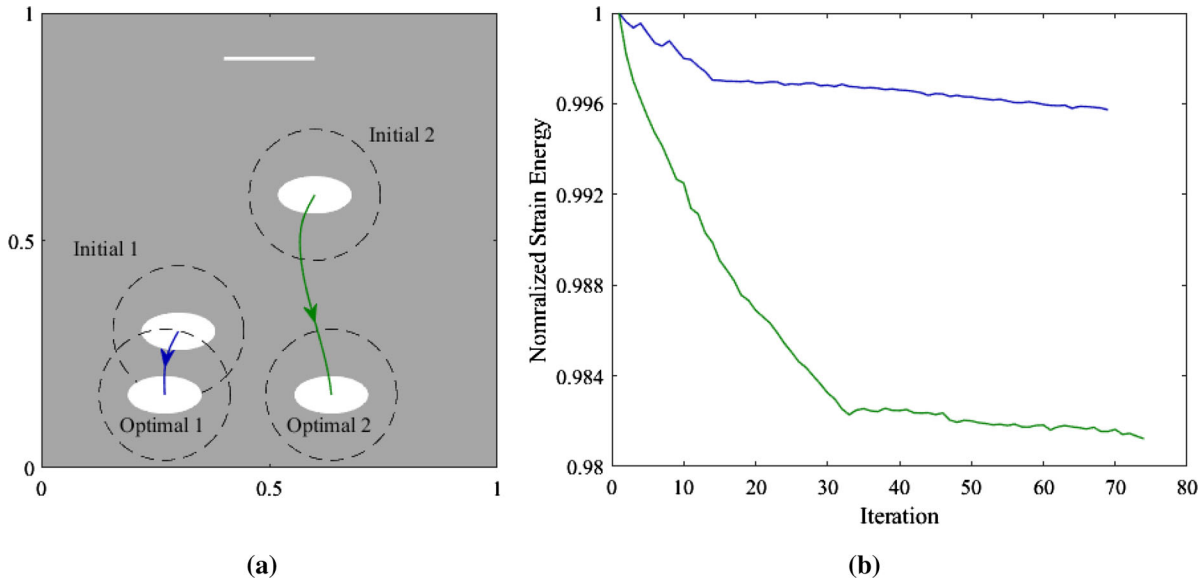

Fig. 9 Optimal configuration obtained by translating an elliptical void inserted into the plate with a crack: **a** Optimal locations of the void starting from different initial locations. **b** Strain energy decrease with iterations

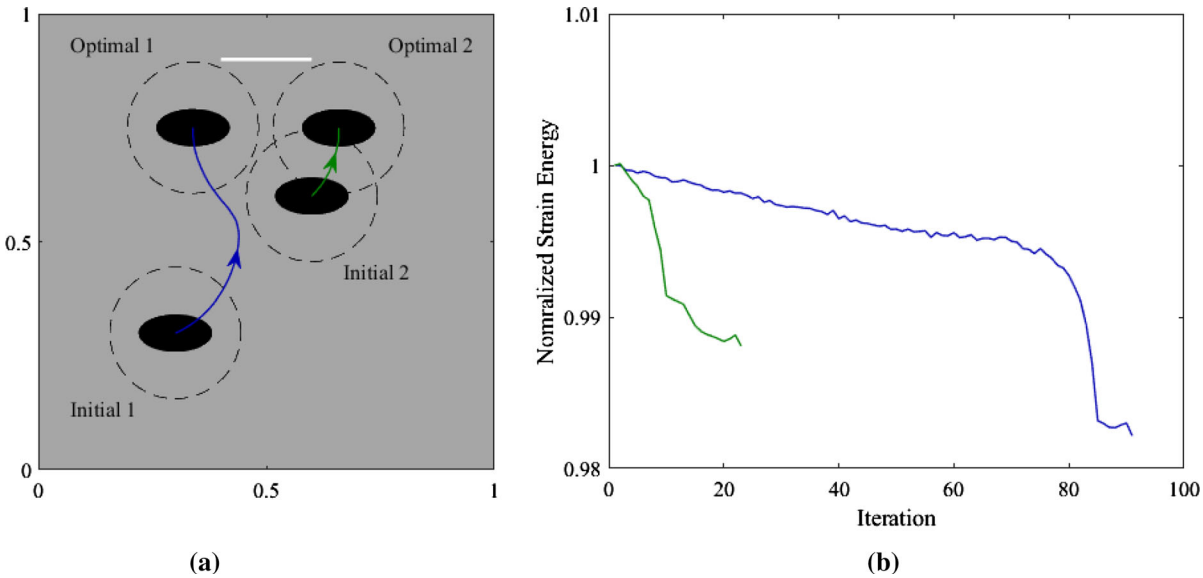

Fig. 10 Optimal configuration obtained by translating an elliptical inclusion inserted into the plate with a crack: **a** Optimal locations of the inclusion starting from different initial locations. **b** Strain energy decrease with iterations

10 Summary

In this study, a configurational optimization problem was proposed for determining the optimal location, orientation, and the scaling of a finite-sized heterogeneity inserted into a homogeneous domain. The material derivative of an arbitrary objective with respect to arbitrary design modifications of the heterogeneity, termed as the configurational derivative, was derived using an adjoint boundary value problem. The configurational derivative was shown to be expressible in terms of a generalized Eshelby energy momentum tensor for arbi-

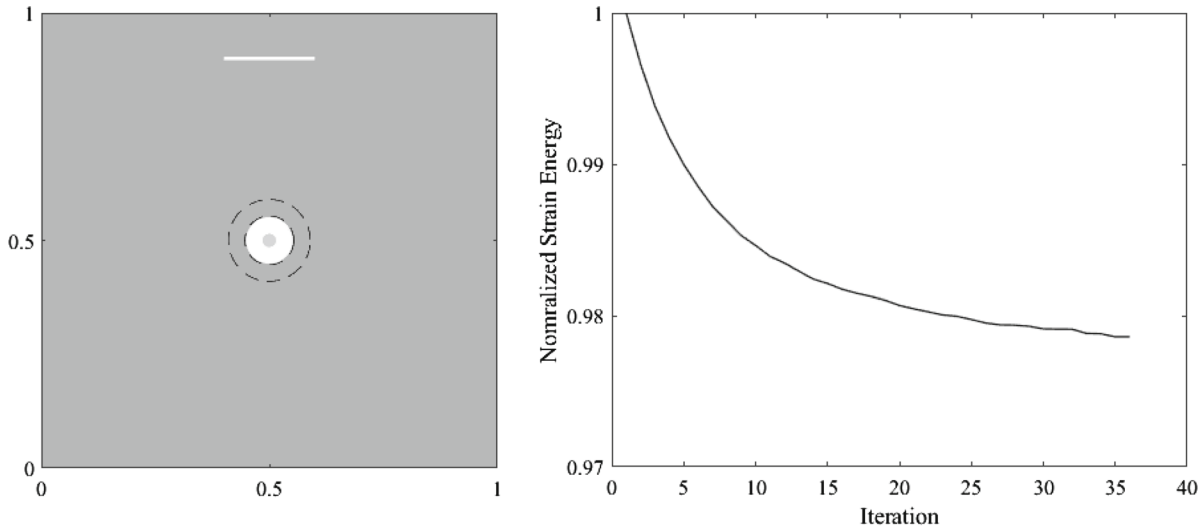

(a) (b)

Fig. 11 Optimal configuration obtained by scaling a circular void inserted into the plate with a crack: **a** Optimal radius of the void - starting from the white circle then shrinking to the gray circle. As before the dashed contour indicates the integration path. **b** Strain energy decrease with iterations

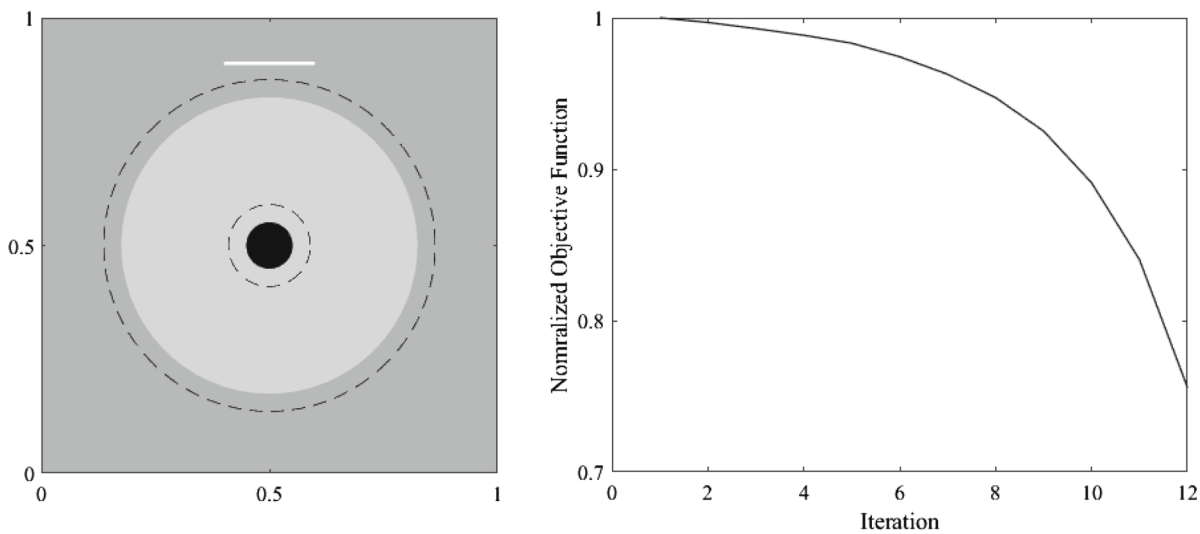

(a) (b)

Fig. 12 Optimal configuration obtained by scaling a circular inclusion inserted into the plate with a crack: **a** Optimal radius of the inclusion - starting from the black circle then expanding to the gray circle. **b** Strain energy decrease with iterations

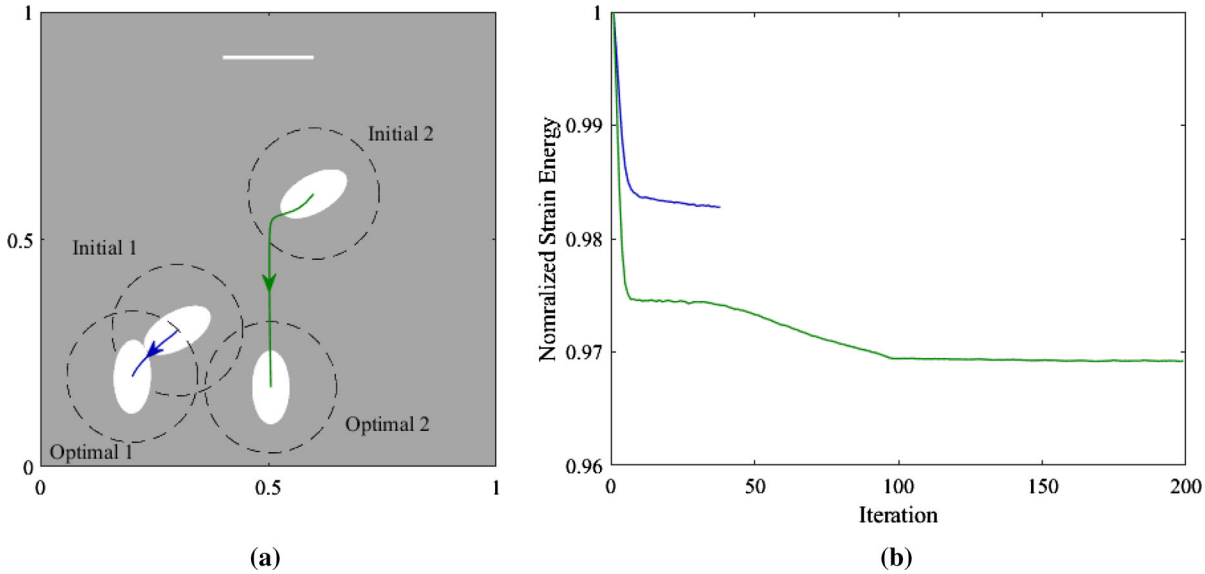

Fig. 13 Optimal configuration obtained by translating and rotating an elliptical void inserted into the plate with a crack: **a** Optimal locations of the void starting from different initial locations. **b** Strain energy decrease with iterations

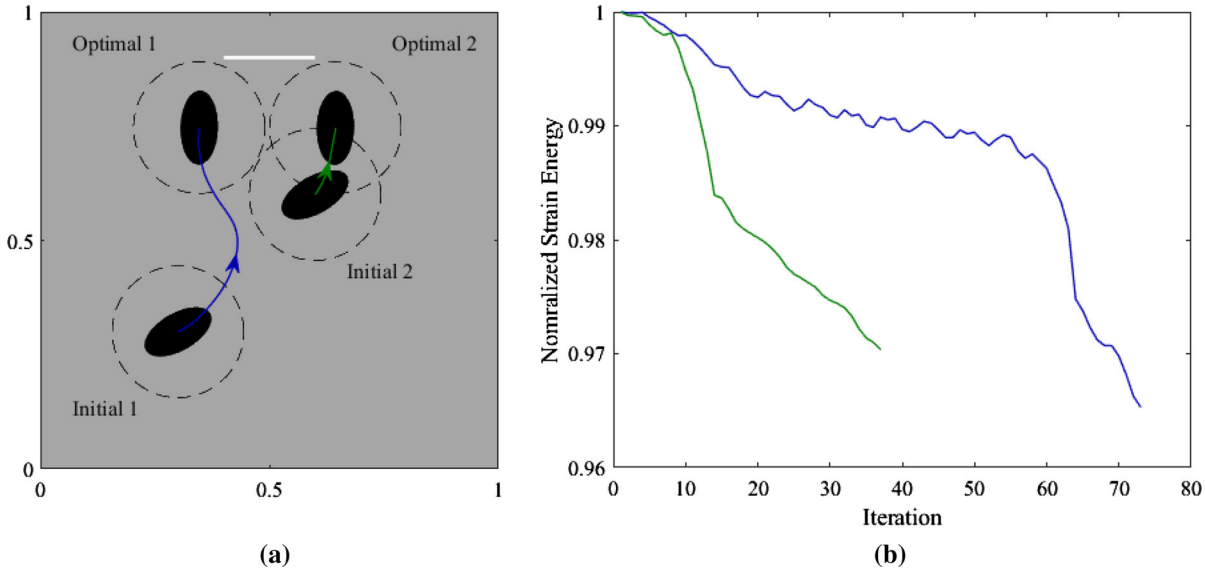

Fig. 14 Optimal configuration obtained by translating and rotating an elliptical inclusion inserted into the plate with a crack: **a** Optimal locations of the inclusion starting from different initial locations. **b** Strain energy decrease with iterations

trary objectives that depended on the solutions to both the original boundary value problem as well as the adjoint boundary value problem. Following the derivation of the configurational derivative, equivalent path-independent integral forms for sensitivity with respect to the general objective for translation, rotation, and scaling of the heterogeneity were derived. The specific forms of the sensitivities for various objective functions, including the strain energy and compliance were derived. The strain energy objective was shown to naturally lead to the $J-$, $L-$ and $M-$integrals of fracture mechanics. The developed theory was implemented in an enriched isogeometric analysis code (EIGA) and several illustrative examples were solved. The first set

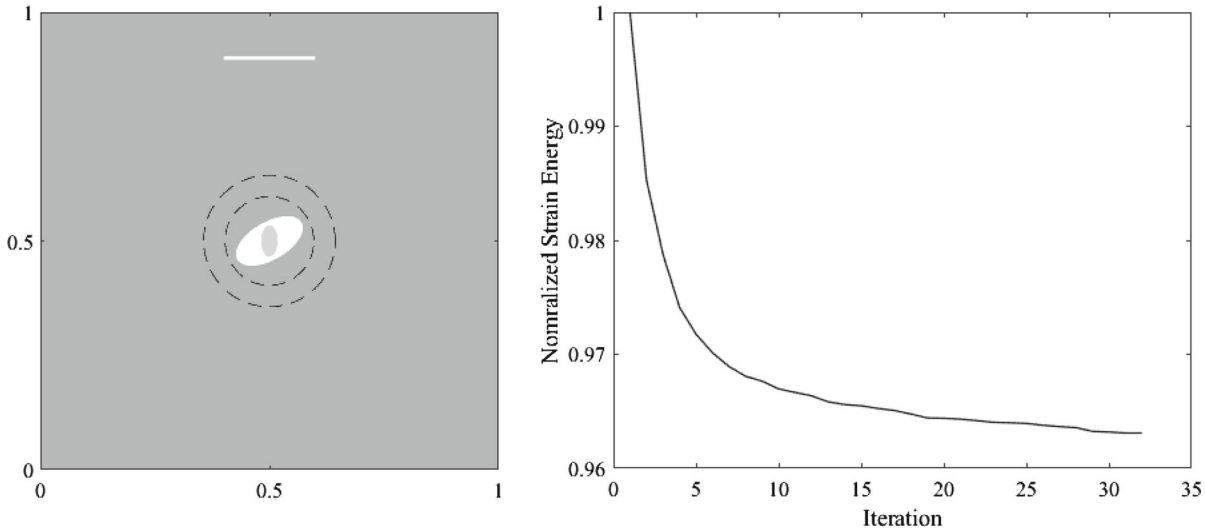

(a) **(b)**

Fig. 15 Optimal configuration obtained by scaling and rotating an elliptical void inserted into the plate with a crack: **a** Optimal configuration of the void - starting from the white ellipse with 30 degree inclination then shrinking to the gray ellipse with 90 degree inclination. **b** Strain energy decrease with iterations

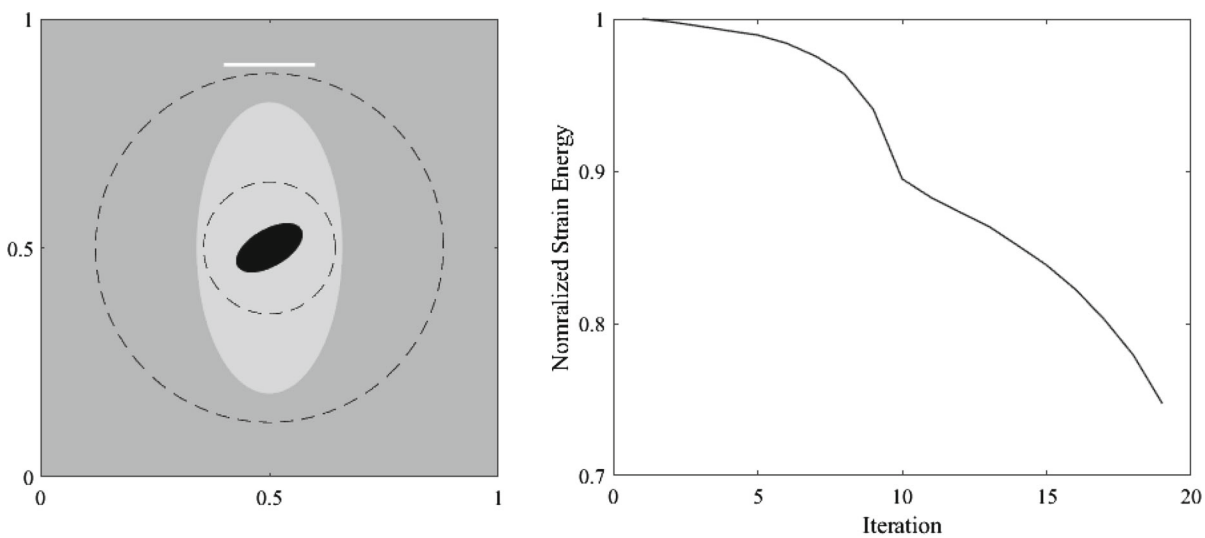

(a) **(b)**

Fig. 16 Optimal configuration obtained by scaling and rotating an elliptical inclusion inserted into the plate with a crack: **a** Optimal configuration of the inclusion - starting from the black ellipse with 30 degree inclination then expanding to the gray ellipse with 90 degree inclination. **b** Strain energy decrease with iterations

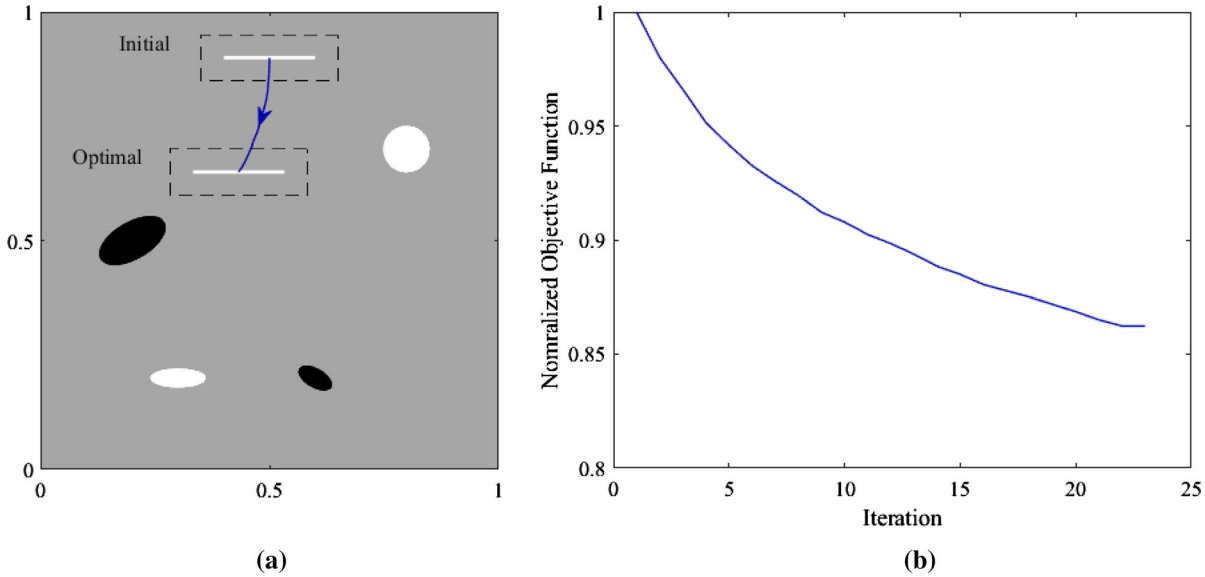

Fig. 17 Optimal location obtained by translating a line crack to minimize the strain energy of the plate while holding the configuration of the voids and inclusions fixed: **a** Optimal location of crack. **b** Strain energy decrease with iterations

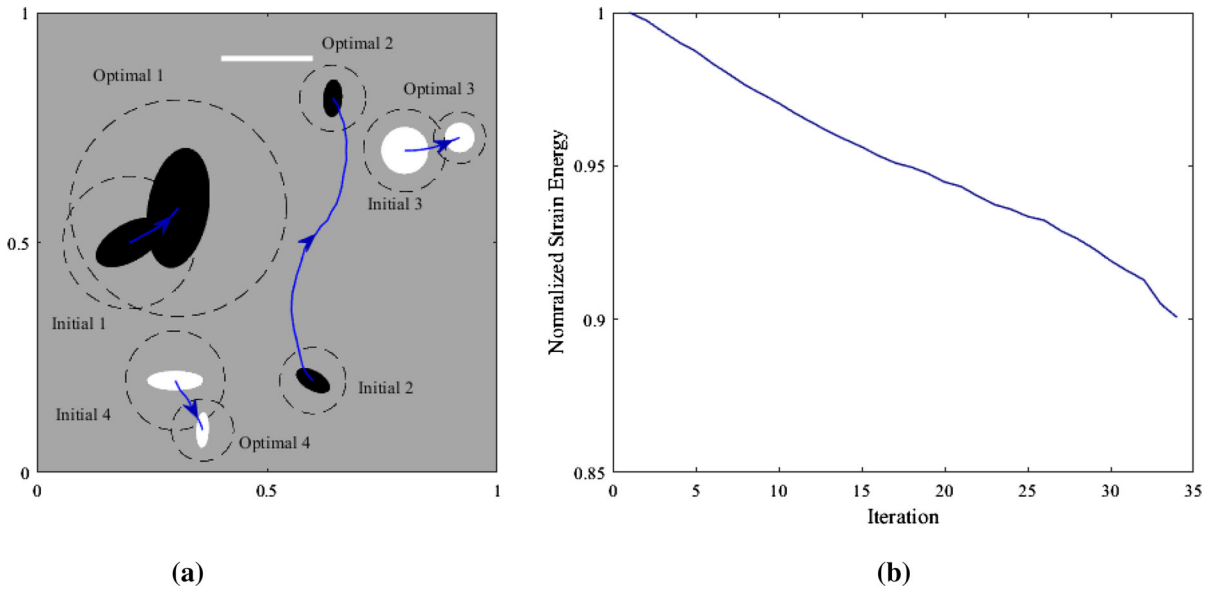

Fig. 18 Optimal configuration of four heterogeneities to minimize the strain energy of the plate with a line crack: **a** Optimal configuration of the four heterogeneities. **b** Strain energy decrease with iterations

of examples identified the worst or best configurations of a horizontal crack with respect to two chosen objectives. Finally, we presented a fracture-resist design strategy that mitigates the risk of fracture by sequentially inserting one or more heterogeneities and optimizing their configuration. While the theory described in the paper is general, any explicit boundary computational method such as the one used in the present study is challenged by the ability to generate complex topologies. The advantage of the computational strategy, however, is its ability to apply sharp interface derivations directly without needing to derive equivalent diffuse interface forms.

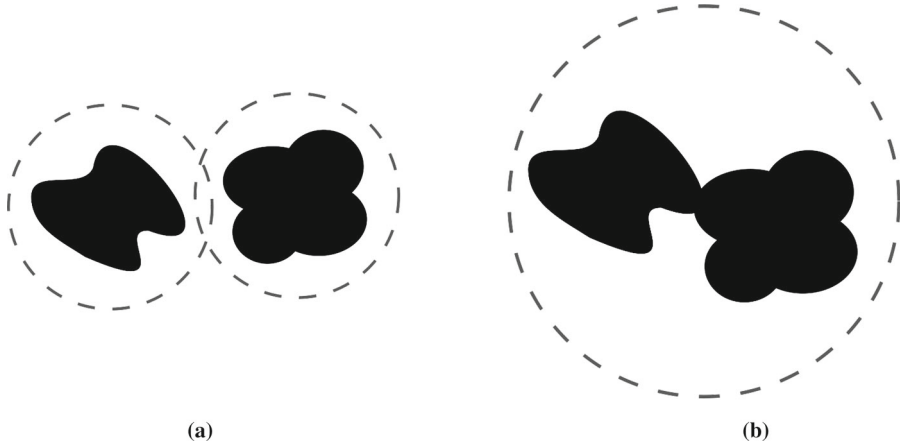

Fig. 19 Merging of heterogeneities: **a** two heterogeneities in close proximity **b** heterogenities post merging to create a larger heterogeneity

Appendix A

A.1 The Divergence of Generalized Eshelby Energy-Momentum Tensor

We derive below the general form of the divergence $\nabla \cdot \mathbf{\Sigma}$ and show that the result reduces to $\nabla \cdot \mathbf{\Sigma} = 0$ if $\mathbf{C}$ and $\mathbf{b}$ are homogeneous in their domains.

$$
\begin{aligned}
\nabla \cdot \mathbf{\Sigma} &= \nabla \cdot \Big[\big(\psi - \boldsymbol{\sigma} : \boldsymbol{\varepsilon}^a + \mathbf{b} \cdot \mathbf{u}^a \big) \mathbf{I} + \boldsymbol{\sigma} \cdot \nabla \mathbf{u}^{aT} + \boldsymbol{\sigma}^a \cdot \nabla \mathbf{u}^T \Big] \\
&= \nabla \psi - \nabla(\boldsymbol{\sigma} : \boldsymbol{\varepsilon}^a) + \nabla(\mathbf{b} \cdot \mathbf{u}^a) + \nabla \cdot (\boldsymbol{\sigma} \cdot \nabla \mathbf{u}^{aT}) + \nabla \cdot (\boldsymbol{\sigma}^a \cdot \nabla \mathbf{u}^T) \\
&= \nabla \psi - \nabla(\boldsymbol{\sigma} : \boldsymbol{\varepsilon}^a) + \nabla(\mathbf{b} \cdot \mathbf{u}^a) + (\nabla \cdot \boldsymbol{\sigma}) \cdot (\nabla \mathbf{u}^{aT}) + \boldsymbol{\sigma} : \nabla(\nabla \mathbf{u}^{aT}) + (\nabla \cdot \boldsymbol{\sigma}^a) \cdot (\nabla \mathbf{u}^T) + \boldsymbol{\sigma}^a : \nabla(\nabla \mathbf{u}^T) \\
&= \nabla \psi - \nabla \boldsymbol{\sigma} : \boldsymbol{\varepsilon}^a - \boldsymbol{\sigma} : \nabla \boldsymbol{\varepsilon}^a + \nabla \mathbf{b} \cdot \mathbf{u}^a + \mathbf{b} \cdot (\nabla \mathbf{u}^{aT}) - \mathbf{b} \cdot (\nabla \mathbf{u}^{aT}) + \boldsymbol{\sigma} : \nabla \boldsymbol{\varepsilon}^a - \mathbf{b}^a \cdot (\nabla \mathbf{u}^T) + \boldsymbol{\sigma}^a : \nabla \boldsymbol{\varepsilon} \\
&= \nabla \psi - \nabla \boldsymbol{\sigma} : \boldsymbol{\varepsilon}^a + \nabla \mathbf{b} \cdot \mathbf{u}^a - \mathbf{b}^a \cdot (\nabla \mathbf{u}^T) + \boldsymbol{\sigma}^a : \nabla \boldsymbol{\varepsilon} \\
&= \frac{\partial \psi}{\partial \mathbf{u}} \cdot \nabla \mathbf{u}^T + \frac{\partial \psi}{\partial \boldsymbol{\varepsilon}} : \nabla \boldsymbol{\varepsilon} - \nabla \boldsymbol{\sigma} : \boldsymbol{\varepsilon}^a + \nabla \mathbf{b} \cdot \mathbf{u}^a - \frac{\partial \psi}{\partial \mathbf{u}} \cdot (\nabla \mathbf{u}^T) + (\mathbf{C} : \boldsymbol{\varepsilon}^a - \frac{\partial \psi}{\partial \boldsymbol{\varepsilon}}) : \nabla \boldsymbol{\varepsilon} \\
&= -\boldsymbol{\varepsilon} : \nabla \mathbf{C} : \boldsymbol{\varepsilon}^a + \nabla \mathbf{b} \cdot \mathbf{u}^a
\end{aligned}
\tag{64}
$$

A.2 Simplification for Rotational Transformation

Rotation is described by $\mathbf{v} = \mathbf{W}\mathbf{x} = \mathbf{w} \times \mathbf{x}$ and $\nabla \mathbf{v} = \mathbf{W}^T$ in Ω_s.

$$\begin{aligned}
&\int_{\Omega_s} \boldsymbol{\Sigma} : \nabla \mathbf{v}\, d\Omega = \int_{\Omega_s} \left(\psi - \boldsymbol{\sigma} : \boldsymbol{\varepsilon}^a + \mathbf{b} \cdot \mathbf{u}^a\right) \mathbf{I} : \mathbf{W}^T\, d\Omega \\
&+ \int_{\Omega_s} \left(\boldsymbol{\sigma} \cdot \nabla \mathbf{u}^{aT}\right) : \mathbf{W}^T\, d\Omega + \int_{\Omega_s} \left(\boldsymbol{\sigma}^a \cdot \nabla \mathbf{u}^T\right) : \mathbf{W}^T\, d\Omega \\
&= \int_{\Omega_s} \left(\boldsymbol{\sigma} \cdot \nabla \mathbf{u}^{aT} + \boldsymbol{\sigma}^T \cdot \nabla \mathbf{u}^a\right) : \mathbf{W}^T\, d\Omega \\
&+ \int_{\Omega_s} \left(\boldsymbol{\sigma}^a \cdot \nabla \mathbf{u}^T + \boldsymbol{\sigma}^{aT} \cdot \nabla \mathbf{u}\right) : \mathbf{W}^T\, d\Omega \\
&+ \int_{\Omega_s} \left[(\nabla \cdot \boldsymbol{\sigma})\, \mathbf{u}^a - \nabla \cdot \left(\boldsymbol{\sigma} \mathbf{u}^a\right)\right] : \mathbf{W}^T\, d\Omega \\
&+ \int_{\Omega_s} \left[\left(\nabla \cdot \boldsymbol{\sigma}^a\right) \mathbf{u} - \nabla \cdot \left(\boldsymbol{\sigma}^a \mathbf{u}\right)\right] : \mathbf{W}^T\, d\Omega \\
&= \int_{\Omega_s} \left(\boldsymbol{\sigma} \cdot \boldsymbol{\varepsilon}^a + \boldsymbol{\sigma}^a \cdot \boldsymbol{\varepsilon}\right) : \mathbf{W}^T\, d\Omega \\
&- \int_{\Gamma_s} \left(\mathbf{t}\mathbf{u}^a + \mathbf{t}^a \mathbf{u}\right) : \mathbf{W}^T\, d\Gamma - \int_{\Omega_s} \left(\mathbf{b}\mathbf{u}^a + \mathbf{b}^a \mathbf{u}\right) : \mathbf{W}^T\, d\Omega
\end{aligned} \tag{65}$$

A.3 Simplification for Scaling Transformation

Scaling results when $\mathbf{v} = \alpha \mathbf{x}$ and $\nabla \mathbf{v} = \alpha \mathbf{I}$ in Ω_s, where α is an expansion parameter.

$$\begin{aligned}
&\int_{\Omega_s} \boldsymbol{\Sigma} : \nabla \mathbf{v}\, d\Omega = \int_{\Omega_s} \Big[\big(\psi - \boldsymbol{\sigma} : \boldsymbol{\varepsilon}^a \\
&+ \mathbf{b} \cdot \mathbf{u}^a\big)\, \mathbf{I} + \boldsymbol{\sigma} \cdot \nabla \mathbf{u}^{aT} + \boldsymbol{\sigma}^a \cdot \nabla \mathbf{u}^T\Big] : \alpha \mathbf{I}\, d\Omega \\
&= \alpha \Bigg[d_m \int_{\Omega_s} \psi\, d\Omega - d_m \int_{\Omega_s} \left(\boldsymbol{\sigma} : \boldsymbol{\varepsilon}^a - \mathbf{b} \cdot \mathbf{u}^a\right)\, d\Omega \\
&+ \int_{\Omega_s} \boldsymbol{\sigma} : \boldsymbol{\varepsilon}^a\, d\Omega + \int_{\Omega_s} \boldsymbol{\sigma}^a : \boldsymbol{\varepsilon}\, d\Omega\Bigg] \\
&= \alpha \Bigg[d_m \int_{\Omega_s} \psi\, d\Omega - d_m \int_{\Gamma_s} \mathbf{t} \cdot \mathbf{u}^a\, d\Gamma \\
&+ \int_{\Gamma_s} \left(\mathbf{t} \cdot \mathbf{u}^a + \mathbf{t}^a \cdot \mathbf{u}\right)\, d\Gamma + \int_{\Omega_s} \left(\mathbf{b} \cdot \mathbf{u}^a + \mathbf{b}^a \cdot \mathbf{u}\right)\, d\Omega\Bigg]
\end{aligned} \tag{66}$$

where, d_m is the problem dimension (2 or 3).

References

Arora J (1993) An exposition of the material derivative approach for structural shape sensitivity analysis. Comput Methods Appl Mech Eng 105(1):41

Arora J, Cardoso J (1992) Variational principle for shape design sensitivity analysis. AIAA J 30:2

Bendsøe MP, Kikuchi N (1988) Generating optimal topologies in structural design using a homogenization method. Comput Methods Appl Mech Eng 71(2):197. https://doi.org/10.1016/0045-7825(88)90086-2

Bennett M, Botkin GMCR (1986) Laboratories, The optimum shape: automated structural design. Plenum Press, New York

Budiansky B, O'Connell R (1976) Elastic moduli of a cracked solid. Int J Solids Struct 12:81

Budiansky B, Rice J (1973) Conservation laws and energy-release rates. J Appl Mech 40:201

Cea J, Garreau S, Guillaume P, Masmoudi M (2000) The shape and topological optimizations connection. Comput Methods Appl Mech Eng 188:713

Chang J, Chien A (2002) Evaluation of M-integral for anisotropic elastic media with multiple defects. Int J Fract 114:267

Chen YH (2001) Ballistic-diffusive heat-conduction equations. Int J Solids Struct 38:3193

Chen CP, Chen Y, Subbarayan G (2021) Singular enrichment for multi-material corners with application to assessing the risk of fracture in semiconductor devices. Eng Fract Mech 248:107739. https://doi.org/10.1016/j.engfracmech.2021.107739

Da D, Qian X (2020) Fracture resistance design through biomimicry and topology optimization. Extreme Mech Lett 40:100890. https://doi.org/10.1016/j.eml.2020.100890

Dems K, Mroz Z (1983) Variational approach by means of adjoint systems to structural optimization and sensitivity analysis-I: variation of material parameters within fixed domain. Int J Solids Struct 19:677

Dems K, Mroz Z (1984) Variational approach by means of adjoint systems to structural optimization and sensitivity analysis-II: structure shape variation. Int J Solids Struct 20:527

Dems K, Mróz Z (1986) On a class of conservation rules associated with sensitivity analysis in linear elasticity. Int J Solids Struct 22(7):737

Eschenauer H, Kobelev V, Schumacher A (1974) Bubble method for topology and shape optimization of structures. Struct Optim 8:42

Eshelby J (1956) The continuum theory of lattice defects. Solid State Phys 3:79

Freund L (1978) Stress intensity factor calculations based on a conservation integral. Int J Solids Struct 14(1):241

Haug V, E.J. and Choi, K.K. and Komkov, (1986) Design sensitivity analysis of structural systems. Design sensitivity analysis of structural systems. Academic Press, Orlando

He M, Hutchinson J (1981) The penny-shaped crack and the plane strain crack in an infinite body of power-law material. J Appl Mech 48:830

Herrmann A, Herrmann G (1981) On energy-release rates for a plane crack. J Appl Mech 48:525

Hughes T, Cottrell J, Bazilevs Y (2005) Isogeometric analysis: CAD, finite elements, NURBS, exact geometry and mesh

refinement. Comput Methods Appl Mech Eng 194(39–41):4135
Irwin G (1957) Relation of stresses near a crack to the crack extension force. In 9th international congress on applied mechanics (University of Brussels), pp. 245–251
Irwin G (1957) Analysis of stresses and strains near the end of a crack traversing a plate. J Appl Mech 24:361
Knowles J, Sternberg E (1972) On a class of conservation laws in linearized and finite elastostatics. Arch Ration Mech Anal 44:187–211
Lin HY, Subbarayan G (2013) Optimal topological design through insertion and configuration of finite-sized heterogeneities. Int J Solids Struct 50(2):429
Luo Y, Subbarayan G (2007) A study of multiple singularities in multi-material wedges and their use in analysis of microelectronic interconnect structures. Eng Fract Mech 74(3):416
Natekar D, Zhang X, Subbarayan G (2004) Constructive solid analysis: a hierarchical, geometry-based meshless analysis procedure for integrated design and analysis. Comput Aid Des 36(5):473
Park J, Earmme Y (1986) Application of conservation integrals to interfacial crack problems. Mech Mater 5(3):261
Pironneau O (1984) Optimal shape design for elliptic systems. Springer, Berlin
Renken F, Subbarayan G (2000) NURBS-based solutions to inverse boundary problems in droplet shape prediction. Comput Methods Appl Mech Eng 190(11–12):1391
Rice J (1968) A path independent integral and the approximate analysis of strain concentration by notches and cracks. J Appl Mech 35:379
Russ JB, Waisman H (2019) Topology optimization for brittle fracture resistance. Comput Methods Appl Mech Eng 347:238. https://doi.org/10.1016/j.cma.2018.12.031
Russ JB, Waisman H (2020) A novel topology optimization formulation for enhancing fracture resistance with a single quasi-brittle material. Int J Numer Methods Eng 121(13):2827. https://doi.org/10.1002/nme.6334
Seweryn A, Molski K (1996) Elastic stress singularities and corresponding generalized stress intensity factors for angular corners under various boundary conditions. Eng Fract Mech 55(4):529
Sokolowski J, Zochowski A (1999) On the topological derivative in shape optimization. SIAM J Control Optim 37(4):1251
Sokolowski J, Zolesio J (1992) Introduction to shape optimization: shape sensitivity analysis. Springer series in computational mathematics. Springer, Berlin
Subbarayan G (1991) Bone construction and reconstruction: A variational model and its applications. Ph.D. thesis, Cornell University, Ithaca, NY
Tambat A, Subbarayan G (2012) Isogeometric enriched field approximations. Comput Methods Appl Mech Eng 245–246:1
Xia L, Da D, Yvonnet J (2018) Topology optimization for maximizing the fracture resistance of quasi-brittle composites. Comput Methods Appl Mech Eng 332:234. https://doi.org/10.1016/j.cma.2017.12.021

Publisher's Note Springer Nature remains neutral with regard to jurisdictional claims in published maps and institutional affiliations.